Physics potential of LHC

S. ASAI

ICEPP, University of Tokyo, 7-3-1 Hongo,
Bunkyo-ku Tokyo, 113-0033

This document describes the physics potential of LHC. Although there are many topics covered at LHC, high mass and high transverse momentum physics are main purpose of LHC. This note is focused on three major topics, Higgs boson(s), Supersymmetry and top quark. ATLAS and CMS collaborations have enormous potential to discover Higgs boson(s) and Supersymmetry, if it exists at mass scale less than about 1 and 2 TeV, respectively. Methods and potentials to determine the properties of these new particles are also summarised.

1 Introduction

The Large Hadron Collider(LHC) project [1] is the major accelerator program at CERN, and it is now under contraction using the existing 26.6 km circumference LEP tunnel. About 1100 units of 8.4 T superconducting dipole magnet (length of the magnetic field is 14.2 m each) will be arranged in the tunnel. Protons are accelerated up-to 7 TeV and collide each other at four collision points. The centre-of-mass energy of pp-system is 14 TeV. The pilot run is scheduled in April 2006, and the first physics run will start in July 2006 [a]. The design luminosity is $10^{34} cm^{-2} s^{-1}$, which is corresponding to 100 fb^{-1} per one year. During the first three years, LHC will be operated with the lower luminosity of about $10^{33} cm^{-2} s^{-1}$ (denoted as "low luminosity run"). Detectors and front-end electronics are firmly required to be radiation hard for these high luminosities. Furthermore, bunches of proton are separated by only 25 ns, then high speed operations and low dead time of response are strongly demanded on the detectors.

Two general-purpose experiments exist, ATLAS [2] and CMS [3], at LHC. The ATLAS (A Toroidal LHC Apparatus) detector is illustrated in Fig. 1, and it measures 22 m high, 44 m long, and weight 7,000 tons. The characteristics of the ATLAS detector are summarised as follows [4]:

- Precision inner tracking system is constituted with pixel, strip of silicon and TRT with 2 T solenoidal magnet. Good performance is expected on the B-tagging and the γ-conversion tagging.

- Liquid Argon electromagnetic calorimeter has fine granularity for space resolution and longitudinal segmentation for fine angular resolution and particle identifications. It has also good energy resolution of about 2% for 100 GeV-e/γ.

- Large muon spectrometer with air core toroidal magnet will provide a precise measurement on muon momenta(about 2% for 100 GeV-μ) even in the forward region.

ATLAS

S. C. Air Core
Toroids

S. C. Solenoid

Hadron
Calorimeters

Forward
Calorimeters

Muon
Detectors

Inner
Detector

EM Calorimeters
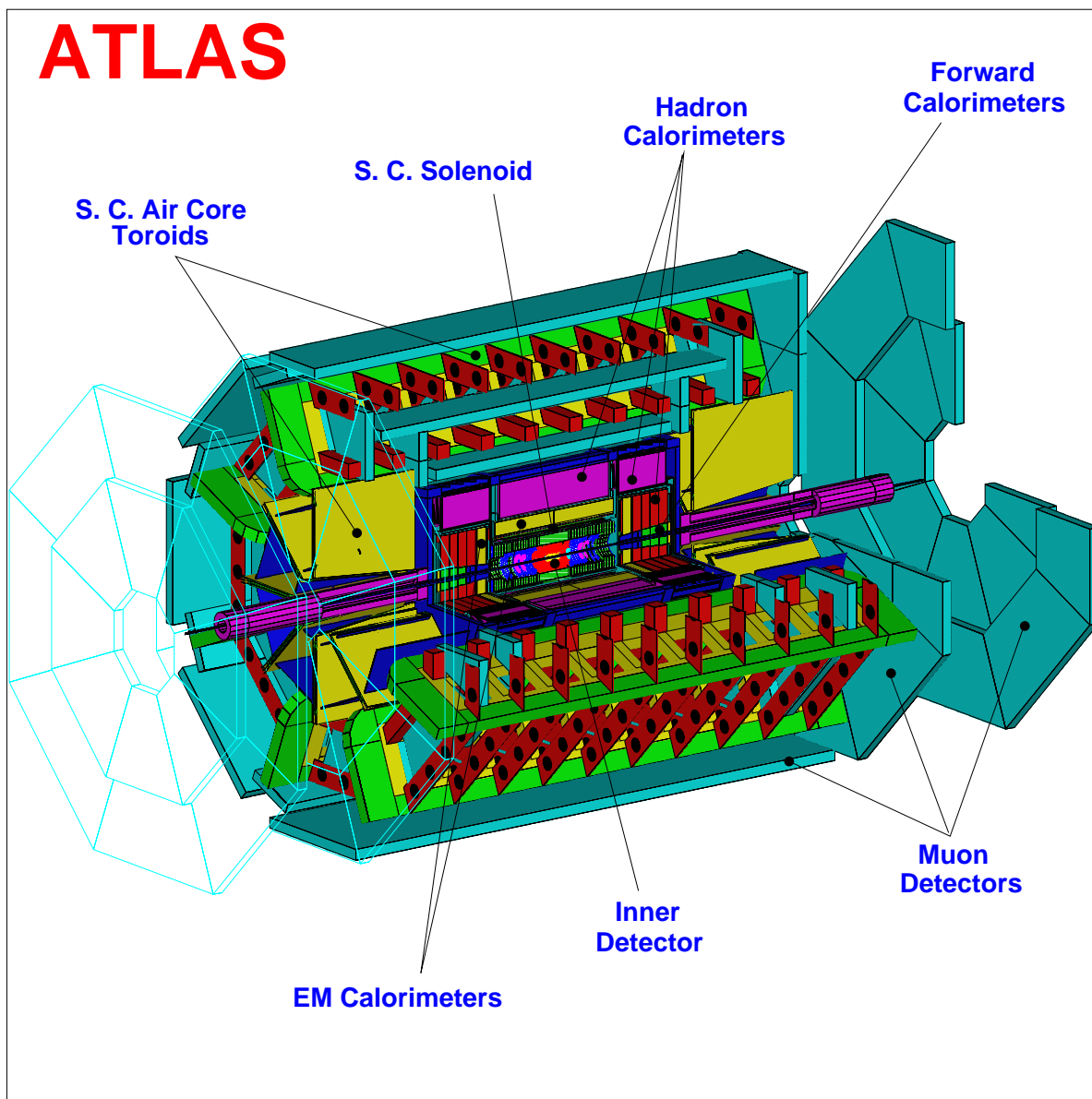
Figure 1: Overall layout of the ATLAS (A Toroidal LHC Apparatus) detector.

Table 1: Event rates for major high p_T and high mass processes with a luminosity of 10 fb^{-1}/year. The expected rates at Tevatron Run-II are also listed, for the comparison. Trigger conditions are not taken into account for these numbers.

	σ (pb)	Rate (Hz)	Event number at LHC(/year)	Event number Tevatron-II (1fb^{-1})
$W^{\pm} \to \ell^{\pm}\nu$	1.7×10^5	170	$\sim 10^9$	$\sim 10^7$
$Z^0 \to \ell^+\ell^-$	2.5×10^4	25	$\sim 10^8$	$\sim 10^6$
$t\bar{t}$	830	0.8	$\sim 10^7$	$\sim 10^4$
$b\bar{b}$ $p_T > 100\text{GeV}$	6,400	6	$\sim 10^8$	
jj $p_T > 200\text{GeV}$	10^5	100	$\sim 10^9$	
SM Higgs (M=115GeV)	35	4×10^{-2}	$\sim 10^5$	$\sim 10^3$
(M=700GeV)	1	10^{-3}	$\sim 10^4$	~ 0
$\tilde{g}\tilde{g}$ (M=500GeV)	~ 100	0.1	$\sim 10^6$	~ 1
(M=1TeV)	~ 1	10^{-3}	$\sim 10^4$	~ 0

The CMS (Compact Muon Solenoid) detector measures 15 m high, 21 m long, and weight 12,500 tons, with the following features[5]:

- Precise measurement on high p_T track is performed with the strong 4 T solenoidal magnet.

- P$bW0_4$ crystal electromagnetic calorimeter is dedicated for $H^0_{SM} \to \gamma\gamma$.

- High purity identification and precise measurement are expected on μ tracks using the compact muon system.

The production cross-sections are expected to be huge at LHC for the various high p_T and high mass elementary processes, since gluon can contribute remarkably even to such processes. Furthermore, LHC provides the high luminosity of 10–100 fb^{-1} per year, the large numbers of the interesting events will be observed as summarised in table 1. LHC has an enormous potential to produce the high mass particles, for example, top quark, Higgs boson and SUSY particles. High performance is also strongly demanded on the computing system to deal with the large size of the data as listed in the table.

2 Higgs physics

The most urgent and important issue of the elementary particle physics is to understand the mechanism of the Electroweak symmetry-braking and origin of mass. Four experiments at LEP have shown very precisely the validity of the Standard model(SM) for the last 10 years. But there is still the missing knowledge about the Electroweak symmetry-braking, which is crucial for the Standard model. The experimental observation of one or several Higgs bosons will give a solution to this important issue. Furthermore, the detail studies on Yukawa couplings between the Higgs boson(s) and various fermions will give insights to the origin of mass. Discovery and the detail studies on the various properties of Higgs boson(s) are the primary subject at LHC, and the most urgent issue of the modern particle physics.

2.1 Standard Model Higgs boson: H^0_{SM}

In the Standard model, one doublet of Higgs field is economically assumed, leading to the existence of one neutral scalar particle (H^0_{SM}). The Higgs boson mass is not theoretically

---

[a]A luminosity of 10fb^{-1} will be integrated until February 2007.

predicted by the model, but it's upper limit is considered to be about 1 TeV, which is obtained from the unitary bound of the W^+W^- scatter.

There are following four relevant production processes of the Higgs boson at LHC, and Fig. 2 shows the cross-section of each process as a function of the H^0_{SM} mass [6].

(a) $gg \to H^0_{SM}$: Gluon fusion process has the leading cross-section(20 pb for M_H=160 GeV), and H^0_{SM} is produced via the heavy quark loops[b]. Since there is no characteristic particle associate-produced with H^0_{SM}, it is difficult to find out Higgs boson decaying into hadron owing to the huge number of the QCD background. Only $H \to \gamma\gamma, ZZ(\to \ell\ell\ell\ell)$ and $W^+W^-(\to \ell\nu\ell\nu)$ decay modes are promising.

(b) $qq \to qq\, H^0_{SM}$: Vector Boson Fusion process has also large cross-section in the wide mass range as shown in Fig. 2. Since the mass of W/Z boson, which are exchanged in t-channel, is 80/91 GeV, the out-going quarks have larger transverse momenta, p_T, than the QCD processes. They will be observed in forward region(Forward jets) [7] with high p_T. Furthermore, there is no colour exchange between two out-going quarks, the Higgs boson will be observed in large rapidity gap. So it is promising channel for the various decay modes of H^0_{SM}.

(c) $q\bar{q} \to W/Z\, H^0_{SM}$: Higgs boson is associate-produced with a vector boson. It will be distinguished from the huge QCD backgrounds, when $W^\pm(Z^0)$ decays into leptons.

(d) $gg, q\bar{q} \to t\bar{t}\, H^0_{SM}$: H^0_{SM} is associate-produced with the top quark pair through large Yukawa coupling of top quark. Although production cross-section is relatively small (0.3 pb for 130 GeV) as shown in the figure, the huge QCD background events can be suppressed with tagging top pair. It is very promising channel for the light Higgs boson ($< 130 \sim 140$ GeV). $gg, q\bar{q} \to b\bar{b}\, H$ process is also possible through the Yukawa coupling of bottom quark, but this channel is very difficult because of the QCD background ($gg \to b\bar{b}b\bar{b}$) for the standard Higgs boson. It becomes very important for the MSSM heavy Higgs bosons with a large value of $\tan\beta$, since the cross-section of $b\bar{b}H$ is enhanced by factor of $(\tan\beta)^2$.

The processes (b) and (c) are governed by the couplings between the Higgs boson and Gauge bosons. On the other hand, (a) and (d) are proportional to square of the Yukawa coupling of heavy quarks. We have a good chance to measure directly the couplings of Higgs boson to various particles with comparison the produced numbers of these processes.

Figure 3 shows the decay branching fraction of H^0_{SM} as a function of Higgs mass [6,8]. H^0_{SM} decays mainly into $b\bar{b}$ and $\tau^+\tau^-$ for the lighter case (<130 GeV). On the other hand, the decays into W^+W^- and ZZ have a large fraction for the heavier case (>140 GeV). Although the decay into $\gamma\gamma$ is suppressed due to one-loop process including heavy quarks, this decay mode has a sizable fraction for the case of (100–130 GeV). As mentioned in section 2.1.1, this decay mode is very important at LHC. Mass of H^0_{SM} is expected to be within $115-200$ GeV with the precision measurements on the standard model processes at LEP [9], then all five decay modes ($b\bar{b}$, $\tau^+\tau^-$, $\gamma\gamma$, W^+W^- and ZZ) are important and should be covered.

2.1.1 $H^0_{SM} \to \gamma\gamma$

The branching fraction of this decay mode is small and there is a large background processes via $q\bar{q}, gg \to \gamma\gamma$. Also the bremsstrahlung process $qg \to \gamma q(\to \gamma q)$ contributes background events. But both ATLAS [4] and CMS [5] detectors have the excellent energy and position resolutions for photon. A mass resolution of $H^0_{SM} \to \gamma\gamma$ process is 1.1 GeV(ATLAS) and 0.6GeV(CMS) at the low luminosity run. It becomes slightly worse to 1.3 GeV(ATLAS) and 0.7GeV(CMS) at the

---

[b]The contribution of the top quark dominates, small contributions (about 5%) comes from the bottom quark.
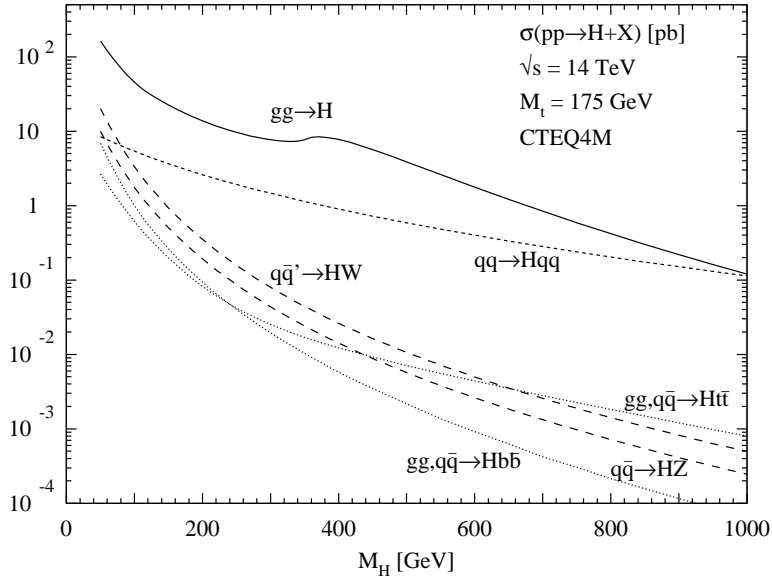
Figure 2: Production cross-section of H^0_{SM} as a function of the mass for the various processes (NLO calculation).
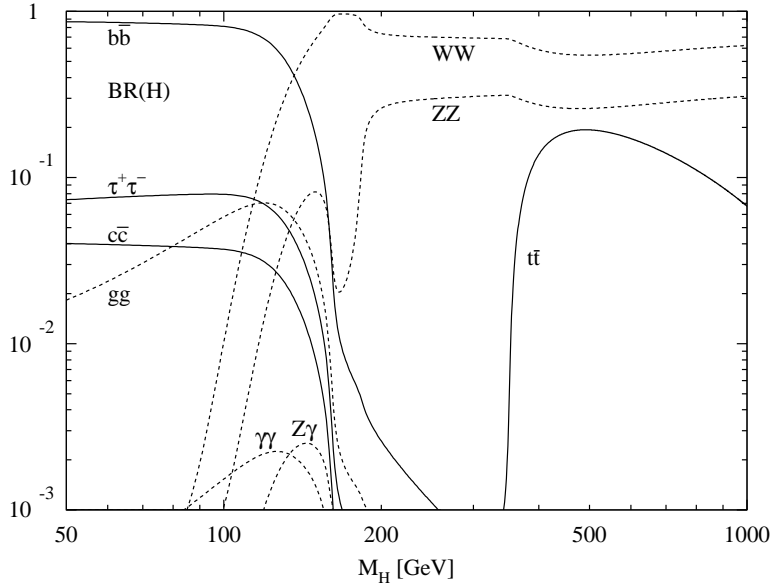
Figure 3: Decay branching fraction of H^0_{SM}.
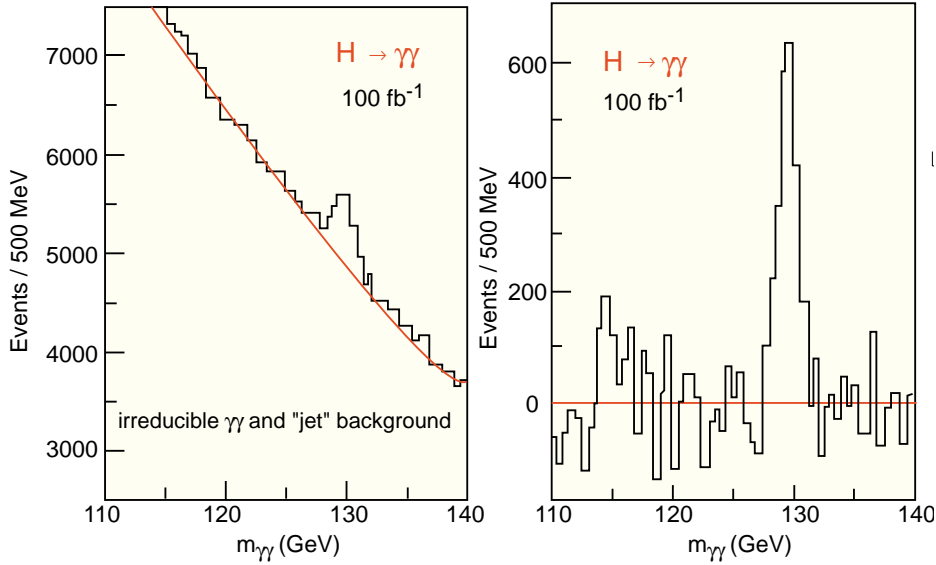
Figure 4: The invariant mass distribution of $\gamma\gamma$ (L=100 fb^{-1} at CMS). M(H$^0_{SM}$)=130 GeV. Left figure shows signal plus background events, and right shows subtracted spectrum. In addition to $\gamma\gamma$ background, there are jet-γ and jet-jet background events.

design luminosity due to the pile up effect[c], but it is still good enough to distinguish the signal from the background events as shown in Fig. 4. Sharp peak appears at Higgs boson mass over smooth distribution of the background events.

Detection efficiency of two isolate γ's is expected to be higher at ATLAS because of the large acceptance and better performance on the identify γ-conversion inside the inner detector. Both detectors have the similar sensitivity to find out H$^0_{SM} \to \gamma\gamma$ process[10]. This channel is promising for the light Higgs boson, whose mass is within 90 and 130 GeV.

2.1.2 $pp \to t\bar{t}\, H^0_{SM}\, (\to b\bar{b})$

The dominant decay mode of H$^0_{SM}$ is to b$\bar{\text{b}}$, when the mass is smaller than 130 GeV. But b$\bar{\text{b}}$ background is enormous as shown in table 1, and it is impossible to separate (and trigger) the H$^0_{SM} \to$ b$\bar{\text{b}}$ signal only. Additional associate-produced particles are necessary to suppress background events and to make sure trigger (for example, W$^\pm$ H$^0_{SM}$ and t$\bar{\text{t}}$ H$^0_{SM}$). Top quark pair has very characteristic event topology, and it provide a high p_T lepton that can be used as trigger. Since signal events contain four bottom quarks, b-tagging plays important role in this channel. The ATLAS detector has three pixel layers at 4,7 and 11 cm from the beam axis, and the tagging efficiency is about 60%[4]. Rejection factors are 100 and 10 for light quarks and charm quark, respectively.

Figure 5 shows the invariant mass distribution of b$\bar{\text{b}}$ after t$\bar{\text{t}}(\to$ bjjb$\ell\nu$) is reconstructed[11]. Peak can be observed at Higgs boson mass with $S/B = 0.73$. Since the production cross-section becomes quickly smaller as Higgs boson is heavier as shown in Fig. 2, the process is promising for $<\sim$ 130 GeV. This channel has also good sensitivity to Yukawa coupling of the top quark, and it can be determined with accuracy of 25% (including systematic error)[12].

---

[c]23 minimal bias events are piled up at the design luminosity.
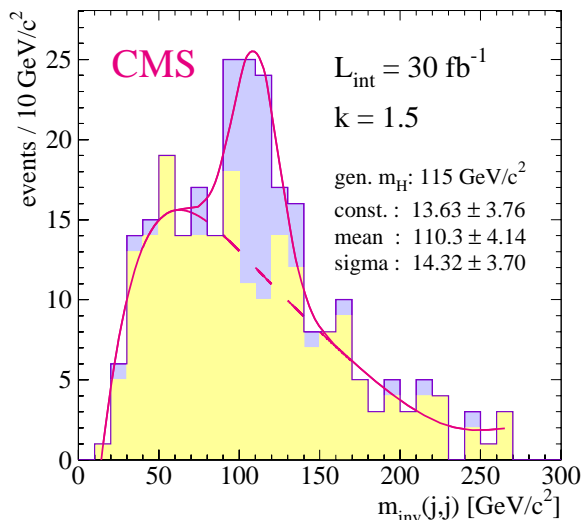
Figure 5: The invariant mass distribution of b$\bar{\text{b}}$ after t$\bar{\text{t}}$($\to$ b$\bar{\text{b}}\ell\nu qq$) is reconstructed (L=30 fb^{-1}). M(H$^0_{SM}$) is assumed to be 115 GeV, and K-factor(1.5) is applied on only the Higgs signal. Dark hatched histogram shows the contribution of signal, and light hatched shows the background distribution.

2.1.3 $qq \to qq\,\text{H}^0_{SM}$: Vector Boson Fusion

The out-going quarks are observed in the forward regions, and have large p_T of about half of W$^\pm$ and Z^0 masses. Tagging these forward jets help us to suppress the background processes. H$^0_{SM} \to \tau^+\tau^-$ provides high p_T $\ell^\pm$ in the case of a leptonic τ-decay, and it can be clearly used as trigger. Momenta carried by ν's emitted from τ decays can be solved approximately using the $\not{E}_T$ information[d], and Higgs mass can be reconstructed even in this case[13]. Typical mass resolutions are about 10 – 13 % depending on the Higgs mass. Careful investigations of this channel are going still under way, but we can expect significance of about 4 σ for this channel for $m_{\text{H}^0_{SM}} < 130\ GeV$ with a luminosity of 30 fb^{-1}.

H$^0_{SM} \to$ W$^+$W$^- \to \ell\nu jj$ provides also high p_T and Higgs mass can be reconstructed using the $\not{E}_T$ information. We hope this channel covers the region of $m_{\text{H}^0_{SM}} > 130\ GeV$, since the branching fraction of H$^0_{SM} \to$ W$^+$W$^-$ increases. Careful investigations of this channel are also going still under way, and the similar significance as H$^0_{SM} \to \tau^+\tau^-$ is expected.

2.1.4 $gg \to$ H$^0_{SM}$ ($\to$ Z$Z \to \ell^+\ell^-\ell^+\ell^-$)

Dominant decay modes of the heavy H$^0_{SM}$ become into ZZ and W$^+$W$^-$ as shown in Fig. 3. Four-lepton channel(H$^0_{SM} \to$ Z$Z \to \ell^+\ell^-\ell^+\ell^-$) is very clean and the gold-plated in these bosonic decays. Although the branching fraction of Z$Z \to \ell^+\ell^-\ell^+\ell^-$ is small, a sharp mass peak is expected as shown in Fig. 6. Mass resolutions of four lepton system are 1.6 and 2.2 GeV for M(H^0_{SM})=130 and 180 GeV, respectively[12]. The $\ell^+\ell^-\ell^+\ell^-$ channel has a good performance in the wide mass range from 130 to 800 GeV, except for 160 GeV. When Higgs mass is 160 GeV, the branching fraction of H$^0_{SM} \to$ W$^+$W$^-$ is almost 100%, and this case is well covered[12] by the other analysis of W$^\pm$H$^0_{SM} \to WWW \to \ell\nu\ell\nu\ell\nu$.

When H$^0_{SM}$ is heavier than 600 GeV, the production cross-section of H$^0_{SM}$ becomes small. Furthermore, a natural decay width[e] of H$^0_{SM}$ becomes larger than 100 GeV, and the mass

---

[d]ν is assumed to emit in the same direction of the observed particles.

[e]Γ(H$^0_{SM} \to VV$) is proportional to m^3(H$^0_{SM}$).
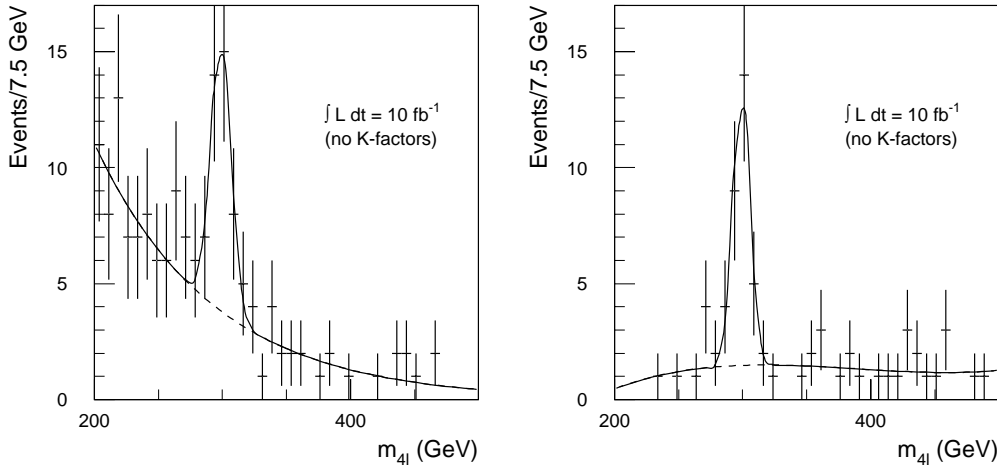
Figure 6: The invariant mass distribution of $\ell^+\ell^-\ell^+\ell^-$ (L=10 fb^{-1} at ATLAS). M(H$^0_{SM}$)=300 GeV. Two Z^0's are reconstructed from four leptons, and the momenta are rescaled using Z^0 mass in order to improve a mass resolution. Right histogram shows the distribution after one of the reconstructed Z^0 is required to have p_T larger than 1/3 Higgs mass. After this selection is applied, the ZZ background events are suppressed and the distribution becomes flat.

peak becomes broad. So there is no benefit to use only leptonic decay of Gauge bosons. and H$^0_{SM} \rightarrow WW \rightarrow \ell\nu jj$ is promising channel [12] for such a heavy case.

2.1.5 Overall discovery potential of H$^0_{SM}$

Discovery potential of H$^0_{SM}$ are summarised in Fig. 7(a) as a function of Higgs mass with an integrated luminosity of 100 fb^{-1}. Only the gold-plated channels mentioned above are used to calculate significance. H$^0_{SM} \rightarrow \gamma\gamma$ and t$\bar{\text{t}}$H$^0_{SM}(\rightarrow$ b$\bar{\text{b}}$) channels have good potential in the mass region between 80 and 130 GeV. A significance combined with both channels is closer to 10σ. The Vector Boson Fusion process is also expected to contribute to large significance in this region, but it is not yet included in the calculation. For heavy case, ($\geq$ 130 GeV), decay to ZZ($\rightarrow \ell^+\ell^-\ell^+\ell^-$) has an excellent performance much higher than 10σ.

Figure 7(b) shows the combined performance [10] of ATLAS and CMS detectors for various luminosities. When the integrated luminosity of each experiment is larger than 10 fb^{-1}, which is corresponding to just one year at the low luminosity run, the significance of H$^0_{SM}$ is larger than 5σ on the all mass region from 115 GeV^f to 1 TeV. **A critical test on the Higgs mechanism can be performed within the first year at LHC.**

2.2   MSSM Higgs bosons

There are three neutral and one charged Higgs bosons, h^0, H^0, A^0 and H$^\pm$, in the minimal supersymmetric model (MSSM), since the supersymmetric models need different Higgs bosons to generate masses for the up- and the down-type fermions. Two parameters are necessary to describe the masses and the couplings of these Higgs bosons at tree level in the MSSM. A mass of A^0 (m_{A^0}) and the ratio of the vacuum expectation values of two Higgs doublet field ($\tan\beta$) are taken, in general, as free parameters [14].

---

^{f}It is current lower bound on the H$^0_{SM}$ mass, obtained at LEP-II.
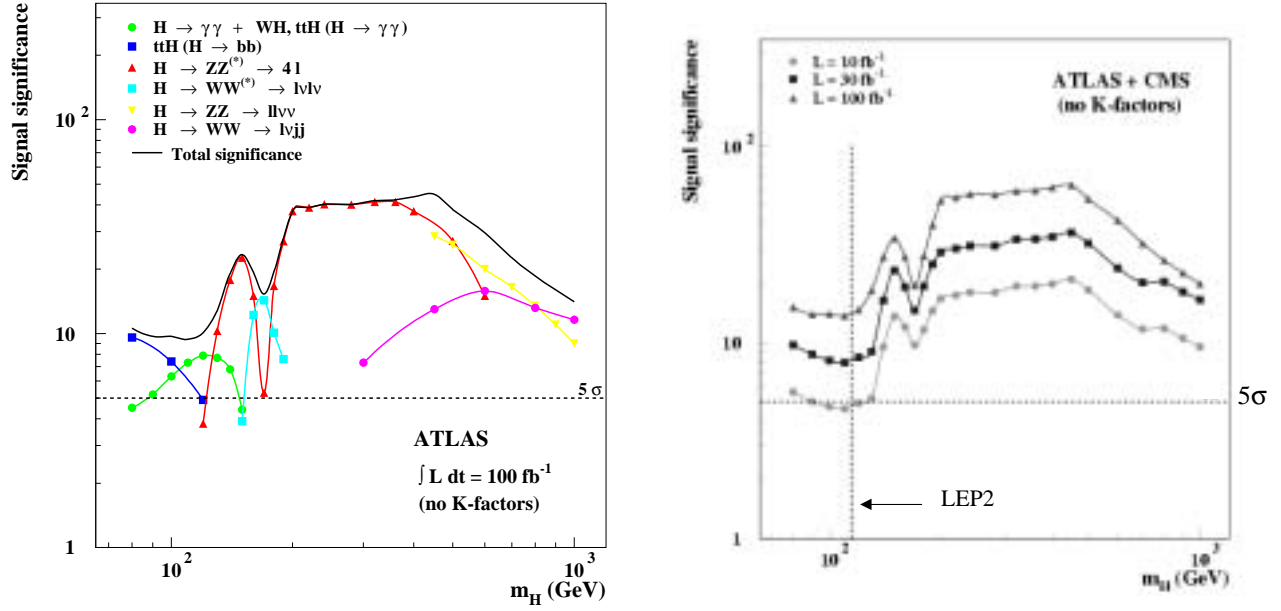
Figure 7: (a)H^0_{SM} discovery potential with L=100 fb^{-1}. Horizontal axis is a mass of Higgs boson, and vertical axis is significance of Higgs signal. Horizontal dotted line shows 5σ. (b) The combined significance of ATLAS and CMS with L=10, 30 and 100 fb^{-1} at each experiment. LEP2 means the current lower-limit (95%C.L.) obtained at all four LEP experiments.

2.2.1 light CP-even Higgs: h^0

The light CP-even Higgs boson, h^0, is expected to be lighter than Z^0 at tree level, but the radiative corrections to the mass (mainly due to $t\bar{t}$ loop) increase this upper-limit up to $\sim$ 130 GeV. If m_{A^0} is larger than 200 GeV, the couplings of h^0 is like those of H^0_{SM} [14]. Then $h^0 \to \gamma\gamma$, $t\bar{t}\,H^0_{SM}\,(\to b\bar{b})$ and Vector Boson Fusion processes have good performances on h^0 as the same as light SM Higgs boson. Figure 8(a) shows 5σ-discovery contour in m_{A^0} and $\tan\beta$ plane. Almost all parameter space is covered by the $t\bar{t}\,H^0_{SM}\,(\to b\bar{b})$ channel, and the $h^0 \to \gamma\gamma$ also contributes at a large value of m_{A^0} [12]. The Vector Boson Fusion process also will contribute to the large parameter space, but it is not yet included in this calculation. Almost all parameter space is covered at LHC except for the small gap around m_{A^0}=100 GeV and $\tan\beta > 8$. This gap is covered by the heavy Higgs boson H and A.

2.2.2 Heavy CP-even Higgs boson and CP-odd Higgs: H^0 / A^0

A mass of the heavy CP-even Higgs boson, H^0, is $\sqrt{m^2_{A^0} + M^2_W}$, and this relation is stable against the radiative corrections. The H^0 is always heavier than the A^0, while H^0 and A^0 are almost degenerate at a large value of $m_{A^0}(> 200\ GeV)$. The couplings of H^0 and A^0 to the down-type fermions are enhanced by a factor of $\tan\beta$ [14]. Thus the coupling between bottom quark and H^0/A^0 becomes $O(1)$ at a large value of $\tan\beta$. The production cross-sections of the associate-production with $b\bar{b}$ becomes huge, and the production processes of $b\bar{b}\,H^0$ and $b\bar{b}\,A^0$ are promising channels. Since the coupling between H^0 and Vector bosons is suppressed at large m_{A^0}, and since the coupling between A^0 and vector bosons is forbidden by CP-conservation, they decay into $b\bar{b}(\sim 91\%)$ and $\tau^+\tau^-(\sim 9\%)$.

$H^0/A^0 \to \tau^+\tau^-$ provides high p_T $\ell^\pm$ in the case of leptonic τ decay, and it can be used as trigger. Momenta carried by ν's emitted from τ decays can be solved approximately using $\not{E}_T$ information, and Higgs mass can be reconstructed as shown in Fig. 9(a). Mass resolution is
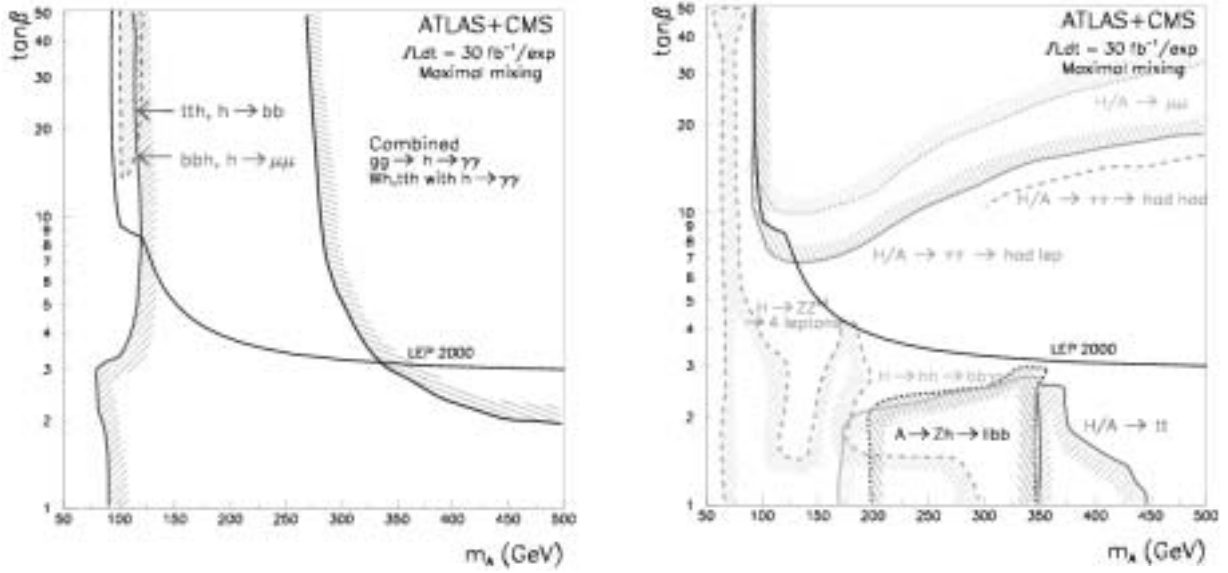
Figure 8: 5σ-discovery contours for (a) h^0 and (b) H^0/A^0. In both figures, LEP2000 means current limits, and significances are calculated with the combination of ATLAS and CMS detector with L=30 fb^{-1} at each experiment.

about 12%, and peak will be observed when $\tan\beta$ is larger than 10. Main background process for $\tau^+\tau^-$ decay is Drell-Yan process, $pp \to \tau^+\tau^- X$, and it can be suppressed after at least one b-jet is required.

The branching fraction to $\mu^+\mu^-$ is much smaller than that into $\tau^+\tau^-$ by factor of $(m_\mu/m_\tau)^2$, whereas the mass resolution of $m_{\mu\mu}$ is expected to be excellent, and clear peak will be observed as shown in Fig. 9(b). Associate-produced b-jet is not required for the $\mu^+\mu^-$ decay, since the signal statistic is limited.

H^0/A^0 will be discovered with more than 5σ C.L., when $\tan\beta$ is larger than about 10 depending on m_{A^0}, as shown in Fig. 8(b). Both decay channels to $\tau^+\tau^-$ and $\mu^+\mu^-$ have the similar potential.

The dominant decay mode of H^0/A^0 is into $b\bar{b}$, which is ten times larger than that into $\tau^+\tau^-$. Although the QCD background is very severe for this channel, the invariant mass of highest two B-jets has a clear peak (mass resolution is about 10%), and it can be seen above continuous distribution comes from the QCD processes. Study is under way with the realistic trigger conditions.

2.2.3 Charged Higgs boson: $H^\pm$

$t \to bH^\pm$ may compete with the standard top decay, $t \to bW^\pm$, if kinematically possible. Such a light $H^\pm$ is corresponding to the small value of m_{A^0}. $H^\pm$ decays into $\tau\nu$ and cs, mainly into $\tau\nu$, when $H^\pm$ is lighter than the top quark, So the $H^\pm$ signal can be observed in the excess of the τ production in the $t\bar{t}$ events.

When $H^\pm$ is heavier than top quark, the dominant decay modes of $H^\pm$ become to tb and $\tau\nu$ depending on $\tan\beta$. At the large value of $\tan\beta$, the branching fraction of $H^\pm \to \tau\nu$ compete with that of $H^\pm \to$ tb, while $Br(H^\pm \to$ tb$)$ is almost 100 % at the small value of $\tan\beta$.

$H^\pm$ is singly produced in $gb \to tH^\pm$ process. This single production processes have a kinematic advantage for heavy $H^\pm$. This signal can be searched for with $H^\pm \to \tau\nu$ plus top quark. τ is identified with a single track, which is well isolated from jet activities, and p_T of the single track is required to be larger than 100 GeV. Figure 10(a) shows the transverse mass
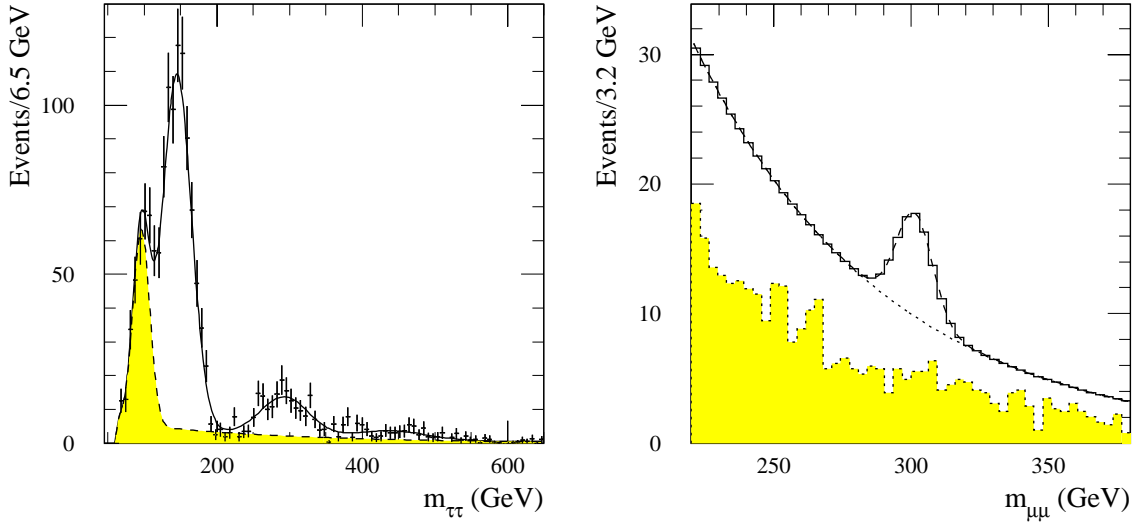
Figure 9: (a) Distribution of $m_{\tau\tau}$ for signals($\tan\beta$=25) plus the background processes with luminosity of 30 fb^{-1}). Open histogram shows the distributions of H^0/A^0 signals (m(A^0)=150,300 and 450 GeV), and the shaded histogram shows the background processes. (b) Distribution of $m_{\mu\mu}$ for the signal($\tan\beta$=30 and m(A^0)=300 GeV) plus background processes.

distribution of the τ candidate and $\not{E}_T$. Signal have the large transverse mass, and it can be separated from the standard model background processes(main contribution comes from the t$\bar{\text{t}}$).

5σ-discovery region for H$^\pm$ is presented in Fig. 10(b). If $\tan\beta$ is larger than 10, the gb $\rightarrow$ t H$^\pm$($\rightarrow \tau\nu$) channel have good performance. Small m_{A^0} region is covered by the exotic decay of top quark mentioned above.

2.3 Measurement of mass and couplings of Higgs boson(s)

Measurements on the properties of the discovered Higgs boson(s) give furthermore insights to the Electroweak symmetry-braking mechanism and to the origin of masses. They are very important works and they maybe open a window of new epoch.

Figures 11 (a) and (b) show the relative precision on the measured mass and decay width of Higgs boson. The standard model Higgs boson is assumed on these studies. As shown in Fig. 11(a), Higgs mass can be measured with an accuracy of less than 0.2%, if the mass is smaller than 500 GeV. When the Higgs boson is heavier than 500 GeV, the resonance of Higgs boson becomes too broad to determine the peak position, and the precision becomes worse. The similar results are obtained on the light MSSM Higgs boson, h^0.

Measurements of the couplings between Higgs boson(s) and fermions/Gauge bosons will give the direct informations of origin of "Mass", and it will give the first evidence of Yukawa couplings. Partial studies on some couplings (for example, top quark[12] and tau[15] Yukawa couplings) have been done, and accuracies of these measured coupling constants are about 10–20%. But more realistic background conditions should be taken into account, and studies are under way now.

3 SUSY physics

Supersymmetric (SUSY) standard models[16] are most promising extensions of the standard model, because the SUSY can naturally deal with the problem of the quadratic Higgs mass divergence. Furthermore, the SUSY models provides a natural candidate for cold dark matter[17], and they have given a hint of the Grand Unification of gauge couplings around 2×10^{16} GeV. In
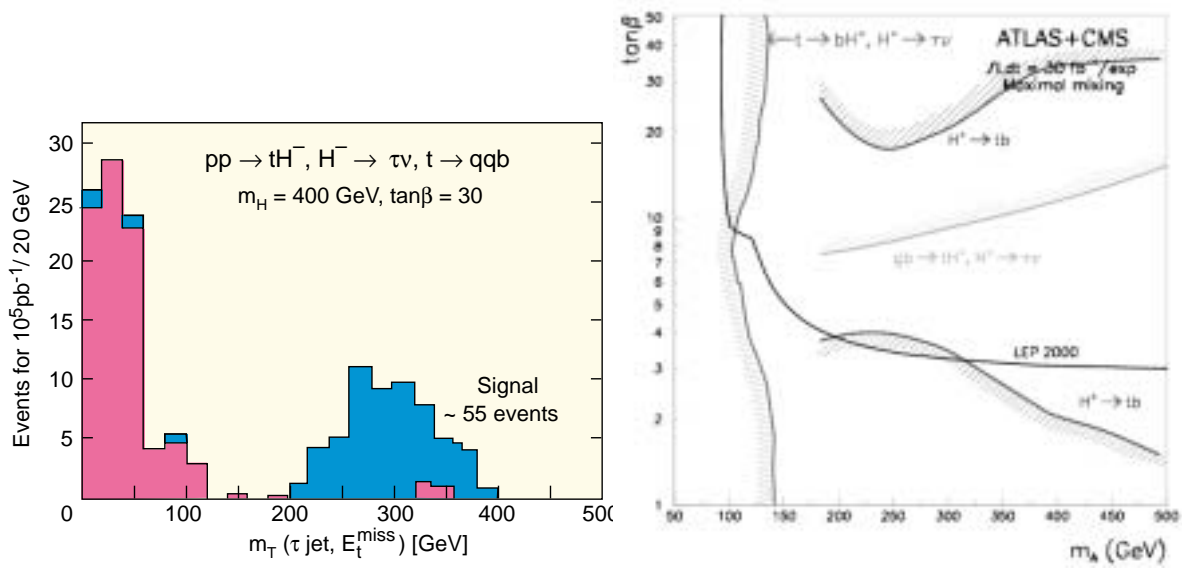
Figure 10: (a) Distribution of transverse mass of τ-jet and $\not{E}_T$ for the H$^\pm$ signal(tan β=40, mass=409 GeV) and the background processes with luminosity of 30 fb^{-1}). (b) 5σ-discovery contour for H$^\pm$.
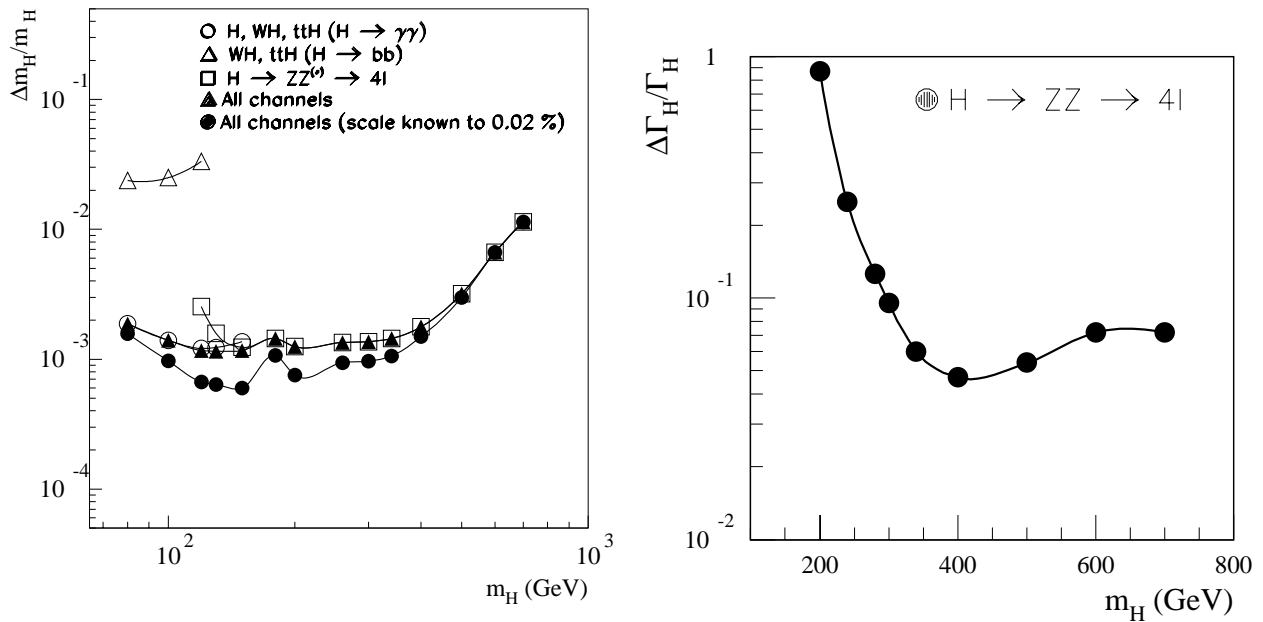
Figure 11: (a) Relative precision on the measured Higgs boson mass as function of Higgs mass with an integrated luminosity is 300 fb^{-1}. The Black triangle and circles correspond to combined all channels with an assumption of uncertainty of 0.1% and 0.02%, respectively, on the absolute energy scale of EM counters. (b) Relative precision on the measured decay width of Higgs boson as function of Higgs boson with L=300 fb^{-1}.

these theories, each elementary particle has a superpartner whose spin differs by 1/2 from that of the particle. Discovery of these SUSY particles should open a window of new epoch, and is one of the important purpose of the LHC project.

There are, in general, more than 100 free parameters to describe SUSY soft breaking [16], following two SUSY models are predictable and promising.

- SuperGravity Model [18] assumes that gravity is responsible for the mediation of the SUSY breaking and provides a natural candidate for cold dark matter [17].

- Gauge-Mediated Model [19] assumes that standard model gauge interactions are responsible for the mediation. It naturally solves the FCNC problem.

Many studies have been performed on these two models and also the other models. Performance based on the SuperGravity model are summarised in this note.

3.1 Introduction of Minimal SuperGravity Model

3.1.1 General introduction

Minimal Super-Gravity Model (mSUGRA) [18] is a special case of the Minimal Supersymmetric Model (MSSM). In this model, the SUSY soft breaking terms are assumed to be communicated from the SUSY breaking sector by gravity. Furthermore, these SUSY soft breaking terms are universal at the GUT scale. There are only five parameters after imposing GUTs conditions;

- m_0: Universal mass of all scalar particles at GUT scale.

- $m_{1/2}$: Universal mass of all gauginos at GUT scale.

- A_0: Common trilinear coupling at GUT scale.

- $\tan\beta(\equiv v_2/v_1)$: Ratio of VEV of two Higgs fields at the Electroweak scale.

- signμ: ± 1, Sign of Higgsino mass term.

Masses of gluino, $\tilde{g}$ and gauginos are mainly determined by $m_{1/2}$. $\tilde{g}$ becomes heavy due to large radiative corrections, and its mass is approximately 2.6 $m_{1/2}$. Higgsino mass ($|\mu|$) becomes larger than gaugino mass at the EW scale, except for the case of $m_0 \gg m_{1/2}$. Then the lighter states of neutralino, $\tilde{\chi}_1^0$ and $\tilde{\chi}_2^0$, become almost pure gaugino states ($\tilde{\chi}_1^0 \sim \tilde{B}^0$, $\tilde{\chi}_2^0 \sim \tilde{W}^0$), and lighter state of chargino, $\tilde{\chi}_1^\pm$, is also gaugino-like ($\tilde{\chi}_1^\pm \sim \tilde{W}^\pm$). Scalar lepton masses are determined mainly by m_0 and weakly by $m_{1/2}$. On the other hand, scalar quark masses depend on both m_0 and $m_{1/2}$.

- $m(\tilde{g}) \sim 2.6\ m_{1/2}$.

- $m(\tilde{\chi}_1^0) \sim 0.4\ m_{1/2}$.

- $m(\tilde{\chi}_2^0) \sim m(\tilde{\chi}_1^\pm) \sim 0.8\ m_{1/2}$.

- $m(\tilde{\ell}_R^\pm) \sim \sqrt{m_0^2 + 0.15 m_{1/2}^2}$

- $m(\tilde{\ell}_L^\pm) \sim \sqrt{m_0^2 + 0.5 m_{1/2}^2}$

- $m(\tilde{q}_{L,R}) \sim \sqrt{m_0^2 + 6 m_{1/2}^2}$

Masses of 3rd generation scalar fermions ($\tilde{t}_1$, $\tilde{b}_1$, and $\tilde{\tau}_1$) depend also on A and $\tan\beta$ [21], and they are generally lighter than first and second generations because of the following two reasons. Firstly, one loop radiative corrections to these masses are always negative, and corrections are proportional to Yukawa coupling. Secondly, the supersymmetric partners of the right-handed and left-handed states mix, and the resultant two mass eigenstates have a large mass splitting. This mixing contribution depends on both A_0 and $\tan\beta$.

3.1.2 Production and Decay processes

Dominant SUSY production processes at LHC are $\tilde{g}\tilde{g}$, $\tilde{g}\tilde{q}$ and $\tilde{q}\tilde{q}$ through the strong interaction. These production cross-sections, σ, do not strongly depend on the SUSY parameters except for masses of $\tilde{g}$ and $\tilde{q}$ [22]. When these masses are 500 GeV, $\tilde{g}\tilde{g}$ is main production process, and total $\sigma(\tilde{g}\tilde{g}$, $\tilde{g}\tilde{q}$ and $\tilde{q}\tilde{q})$ is 100 pb. σ becomes 3 pb for $m_{\tilde{q}}=m_{\tilde{g}}=1$TeV. Even when these masses are 2 TeV, sizable production cross-section of about 20 fb is expected. $\tilde{u}\tilde{u}$ and $\tilde{u}\tilde{d}$ are main production processes for such a heavy case, since u and d quarks are valence quarks. K-factors are about 1.4 [23] for the $\tilde{g}\tilde{g}$, $\tilde{g}\tilde{q}$ and $\tilde{q}\tilde{q}$ production processes (virtual effect), and it is modest value as same as the case of Higgs boson. But all studies presented in this document are based on Leading Order Monte Calro simulations [24,25].

Decay modes of $\tilde{g}$ and $\tilde{q}$ are controlled by the mass-relation between each other, and are summarised in table 2. If kinematically possible, they decay into 2-body through the strong interaction. Otherwise, they decay into a Electroweak gaugino plus quark(s). Bino/Wino-eigenstates presented in this table become simply mass-eigenstate, ($\tilde{B}^0 \sim \tilde{\chi}_1^0$, $\tilde{W}^0 \sim \tilde{\chi}_2^0$, and $\tilde{W}^\pm \sim \tilde{\chi}_1^\pm$), when m_0 is not too larger than $m_{1/2}$. In this case, Higgsino mass ($|\mu|$) becomes larger than gaugino mass at the EW scale, then Higgsino component decouples from lighter mass-eigenstates as already mentioned. Decay modes of third generation squarks ($\tilde{t}_1$ and $\tilde{b}_1$) are more complicated, since they have enough coupling to Higgsino due to non-negligible Yukawa couplings.

Table 2: Decay modes of $\tilde{g}$ and $\tilde{q}$ of 1st and 2nd generations. Branching fractions of $\tilde{g} \to t\tilde{t}$ and $\tilde{g} \to b\tilde{b}$ depend strongly on mass-relation between $\tilde{g}$ and $\tilde{t}/\tilde{b}$.

	$m_{\tilde{q}} > m_{\tilde{g}}$	$m_{\tilde{q}} \sim m_{\tilde{g}}$	$m_{\tilde{q}} < m_{\tilde{g}}$
$\tilde{g}$	$\tilde{g} \to q\bar{q}\tilde{B}^0\ (\sim 1)$ $q\bar{q}\tilde{W}^0\ (\sim 2)$ $q\bar{q}\tilde{W}^\pm\ (\sim 4)$		$\tilde{g} \to q\tilde{q}$
	$\tilde{g} \to t\tilde{t}$ $b\tilde{b}$		
$\tilde{q}_R$	$\tilde{q}_R \to q\tilde{g}$	$\tilde{q}_R \to q\tilde{B}^0$	
$\tilde{q}_L$	$\tilde{q}_L \to q\tilde{g}$	$\tilde{q}_L \to q\tilde{W}^0\ (\sim 1)$ $q\tilde{W}^\pm\ (\sim 2)$	

There are four leading decay modes of $\tilde{\chi}_2^0$ depending on mass spectrum. These are summarised in table 3 with the conditions of mass spectrum. When the scalar lepton, $\tilde{\ell}^\pm$, is lighter than $\tilde{\chi}_2^0$, 2-body decay chain, $\tilde{\chi}_2^0 \to \ell\tilde{\ell}^\pm(\to \ell\tilde{\chi}_1^0)$ becomes dominant decay mode. Branching fraction of $\tilde{\chi}_2^0 \to \tau\tilde{\tau}_1$ is significant large in the case of $\tan\beta \gg 1$. $\tilde{\chi}_2^0 \to h\tilde{\chi}_1^0$ is dominant mode, if the mass difference between $\tilde{\chi}_2^0$ and $\tilde{\chi}_1^0$ is larger than Higgs boson mass. When the mass difference is smaller than m_{Z^0}, three body decay is main decay process. $\tilde{\chi}_1^\pm$ has three leading decay modes, $\tilde{\chi}_1^\pm \to \tilde{\ell}^\pm\nu$, $W^\pm\tilde{\chi}_1^0$ and $f\bar{f}'\tilde{\chi}_1^0$ as the similar manner to $\tilde{\chi}_2^0$.

Table 3: Summary of decay modes of $\tilde\chi_2^0$

decay mode	condition and remarks
$\tilde\chi_2^0 \to \tilde\ell^\pm \ell$	$m_{\tilde\ell^\pm} < m_{\tilde\chi_2^0}$
$\quad \to \ell\tilde\chi_1^0$	(Remarks) $\tilde\chi_2^0 \to \tilde\tau\tau$ for $(\tan\beta \gg 1)$
$\tilde\chi_2^0 \to h\tilde\chi_1^0$	$m_{\tilde\chi_2^0} - m_{\tilde\chi_1^0} > m_h$
$\tilde\chi_2^0 \to Z^0\tilde\chi_1^0$	$m_h > m_{\tilde\chi_2^0} - m_{\tilde\chi_1^0} > m_{Z^0}$
$\tilde\chi_2^0 \to f\bar f\tilde\chi_1^0$	3-body decay, other cases

3.2 Event topologies of mSUGRA events and discovery potential

$\tilde g$ and/or $\tilde q$ are copiously produced at the LHC with $p_T \sim$ M. High p_T jets are emitted from the decays of $\tilde g$ and $\tilde q$ as shown in table 2. Each event contains two $\tilde\chi_1^0$'s in the final state. If R-parity [20] is conserved, $\tilde\chi_1^0$ is stable, and it is neutral and weakly interacting and escape from the detection. Then missing transverse energy, $\not{E}_T$, carried away by two $\tilde\chi_1^0$'s plus multiple high p_T jets is the leading experimental signature of SUSY. Also the other activities of additional jets, leptons and $b\bar b$ are possible, coming from the decays of $\tilde\chi_2^0$ and $\tilde\chi_1^\pm$. These additional informations are important to confirm SUSY signals, and to investigate its properties.

The following four standard model processes can potentially have $\not{E}_T$ event topology with jets.

- $W^\pm$ + jets, $W^\pm \to \ell\nu$

- Z^0 + jets, $Z^0 \to \nu\bar\nu, \tau^+\tau^-$

- $t\bar t$

- QCD jets with mismeasurement

SUSY signals should be observed as an excess of these standard model processes. Large significance can be obtained for SUSY signals after large $\not{E}_T$ and p_T are respectively required on event and jets. $\not{E}_T + \sum_{jets} p_T$ is a good variable [12] to see an excess coming from the SUSY signals as shown in Fig. 12. The distribution of $\not{E}_T + \sum_{jets} p_T$ has steep slop for the standard model background processes as shown in this figure. On the other hand, the distribution for the SUSY signals has a peak at large value, and long tail contribute to the higher side. The shape quite differs from that of the background processes. This peak position has a good sensitivity to $min(m(\tilde g), m(\tilde q))$, and it can be determined with accuracy of 15% [26] using this variable. It will be discussed later. Independent excesses are also expected in the other topologies, for example, $\not{E}_T$ + jets + isolated lepton(s). This isolated lepton will be emitted from $\tilde\chi_2^0$ and $\tilde\chi_1^\pm$.

Figure 13 shows 5σ-discovery potential in m_0-$m_{1/2}$ plane for $\tan\beta = 35$ using the $\not{E}_T$ plus jets channel with various integrated luminosities. Mass contours for $\tilde g$ and $\tilde q$ are also superimposed. As shown in this figure, $\tilde g$ and $\tilde q$ can be discovered close to $M \sim 1.5$ TeV with a luminosity of 1 fb^{-1}, which is corresponding to just one month run with $10^{33} cm^{-2} s^{-1}$. The interesting region for relic density of the dark matter is almost covered with just 1 fb^{-1}. $\tilde g$ and $\tilde q$, whose masses are about 2.5 TeV, can be discovered finally with a luminosity of 300 fb^{-1}. This luminosity is corresponding to three years run with design luminosity of $10^{34} cm^{-2} s^{-1}$. **Both ATLAS [12] and CMS [27] collaborations have an excellent potential to discover SUSY, and they will cover interesting parameter region predicted by naturalness [16] and relic density of dark matter [16,17].**
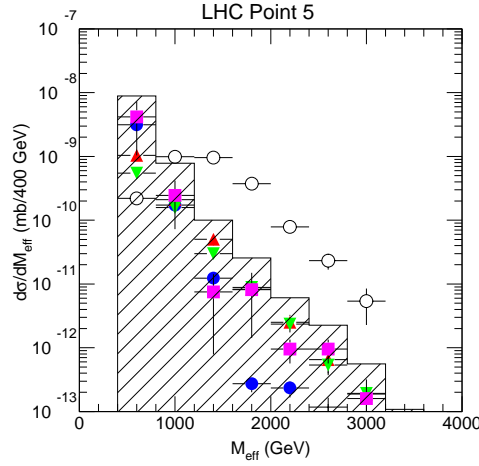
Figure 12: $\not{E}_T + \sum_{jets} p_T$ distributions: (open circles) for SUSY signals at LHC point 5, and (histogram) for sum of all standard model backgrounds. It includes the followings: $t\bar{t}$(black circles), $W^\pm$ + jets(triangles), Z^0 + jets(downward-triangles), and QCD(squares).

3.3   Measurements of masses of SUSY particles

Since two undetected LSP's exist in each event, there are six unknown momentum components in addition to the $\tilde{\chi}_1^0$ mass. So no mass peak is expected in general. However it is possible to use kinematic end points of various distributions as follows [12,27].

- (1) Select specific decay chain exclusively. For example,

$$\begin{aligned}
\tilde{g} &\to \tilde{q}_L q \\
&\to \tilde{\chi}_2^0 q \\
&\qquad \to \tilde{\ell}^\pm \ell \\
&\qquad\qquad \to \tilde{\chi}_1^0 \ell
\end{aligned}$$

- (2) Make various distributions of invariant masses and p_T.

- (3) kinematic constraints are obtained from edges and end points of these distributions. These edges and end points are combinations of the masses, and these are just determined by the kinematics and not depend on the other SUSY parameters.

If there are at least three 2-body decays like this example, full reconstruction of masses is possible model-independently. It is important remark. When we can not find out such three 2-body decays, number of obtained constraint is less than number of unknown masses. Some assumption is necessary to determine mass spectrum of SUSY. SUSY events become background itself for detailed study, since there are many cascade decay patterns in $\tilde{q}$ and $\tilde{g}$.

3.3.1 Kinematic edges for $\tilde{\chi}_2^0$ decay:

$\tilde{\chi}_2^0 \to \ell\tilde{\ell}^\pm (\to \ell + \tilde{\chi}_1^0)$ is the dominant decay mode, when $\tilde{\ell}^\pm$ is lighter than $\tilde{\chi}_2^0$. This is corresponding to the parameter space of $m_0 < \sim 0.8 m_{1/2}$.

The same flavour opposite charge di-lepton($\ell = $ e, μ) is the characteristic signal. Figure 14(a) shows invariant mass distribution of the di-lepton system. Flavour subtraction, $e^+ e^- + \mu^+ \mu^- -$
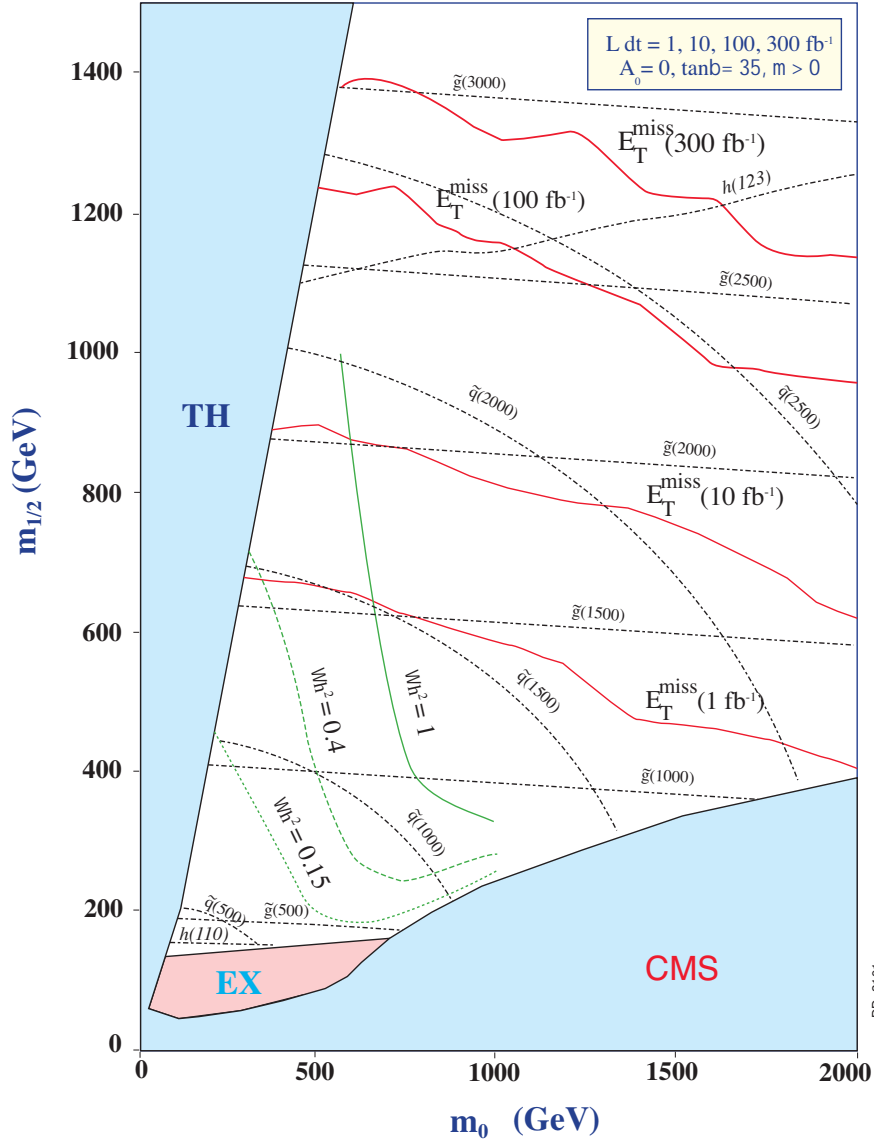
Figure 13: 5σ-discovery region in m_0-$m_{1/2}$ plane for $\tan\beta = 35$ using the $\rlap{/}{E}_T$ plus jets channel. Mass contours for $\tilde{g}$ and $\tilde{q}$ are also superimposed. Ωh^2 shows relic density of the dark matters. In the gray region, $\tilde{\ell}^{\pm}$ becomes the LSP, or no Electroweak symmetry breaking occurs.
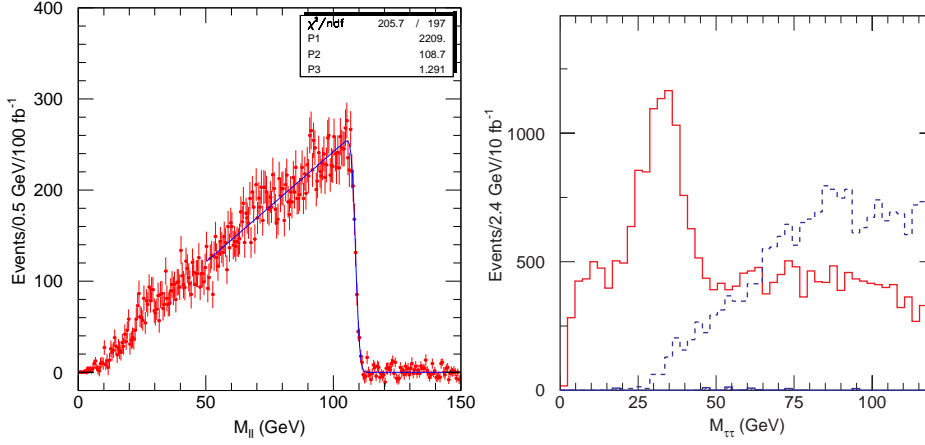
Figure 14: (a) Invariant mass distribution for the di-lepton system (e^+e^- and $\mu^+\mu^-$) (at LHC point 5). Flavour subtraction, $e^+e^- + \mu^+\mu^- - e^+\mu^- - e^-\mu^+$, has been performed. (b) Invariant mass distribution for identified τ-pair system(at LHC point 6). Solid line shows distribution for the correct τ-pair, and dotted line shows the contribution from fake τ.

$e^+\mu^- - e^-\mu^+$, has been performed to suppress flat distribution comes from chargino and $t\bar{t}$ decays. Sharp edge ($M_{\ell\ell}^{max}$) is observed, and it is related to

$$M_{\ell\ell}^{max} = m(\tilde{\chi}_2^0)\sqrt{1 - (m(\tilde{\ell}^\pm)/m(\tilde{\chi}_2^0))^2}\sqrt{1 - (m(\tilde{\chi}_1^0)/m(\tilde{\ell}^\pm))^2}. \tag{1}$$

This can be determined very precisely. Statistical error is 0.1% with L=100 fb^{-1} for this case (it strongly depends on $\sigma \times Br$), and systematic error is less than 0.1%, mainly comes from uncertainty of the energy scale calibration. Figure 15 shows the parameter region in which $M_{\ell\ell}^{max}$ can be determined. $M_{\ell\ell}^{max}$ originated from 2-body decay ($\tilde{\chi}_2^0 \to \tilde{\ell}_L\ell$ and $\tilde{\chi}_2^0 \to \tilde{\ell}_R\ell$) can be observed in a wide region as presented in this figure.

Furthermore, an asymmetry of p_T of two leptons,

$$A_{\ell\ell} = \frac{p_T^{max} - p_T^{min}}{p_T^{max} + p_T^{min}}, \tag{2}$$

has also information on $\tilde{\ell}^\pm$ mass [28]. As $\tilde{\ell}^\pm$ mass is heavier, asymmetry, $A_{\ell\ell}$, becomes larger. Above two kinematic constraints are obtained from the di-lepton system.

When $\tan\beta$ is much larger than 1, $\tilde{\tau}_1$ becomes much lighter than $\tilde{e}_R$ and $\tilde{\mu}_R$, and $\tilde{\chi}_2^0 \to \tilde{\tau}_1\tau$ can become dominant decay mode [29]. Hadronic decay mode of τ is used for a τ-identification. The followings are essence of the τ-identification, and the selection efficiency is about 40%:

- 1-3 prong is selected.

- Energy deposited in calorimeter and these tracks are well concentrated in narrow cone(R=0.2).

- This activity are well isolated from jet activities.

Figure 14(b) shows $M_{\tau\tau}$ distribution, which is visible invariant mass of $\tau\tau$ system times 1/0.66. This factor is mean value to correct the energy carried by neutrinos. Flat contribution in this distribution comes from $\tilde{\chi}_1^\pm \to \tilde{\tau}\nu$. Kinematic edge can be also observed even in the τ case, and this can be determined with accuracy of about 5%. This edge is related to various masses in eq.(1).

$\tilde{\chi}_2^0 \to h\tilde{\chi}_1^0$ becomes the dominant decay mode, when $\tilde{\ell}^\pm$ is heavier than $\tilde{\chi}_2^0$ and the mass difference between $\tilde{\chi}_2^0$ and $\tilde{\chi}_1^0$ is larger than m_h. It is corresponding to the parameter space of
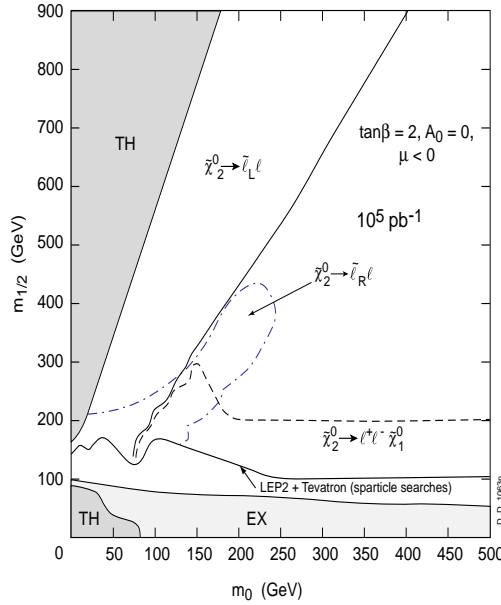
Figure 15: Parameter region for observing the edge of $M_{\ell^+\ell^-}$ due to $\tilde{\chi}_2^0 \to \tilde{\ell}_L\ell$(solid), $\tilde{\chi}_2^0 \to \tilde{\ell}_R\ell$(dashed-dotted) and $\tilde{\chi}_2^0 \to \ell^+\ell^-\tilde{\chi}_1^0$(dashed).

0.4 $m_{1/2} > m_h$. Fig. 16(a) shows the $M_{b\bar{b}}$ distribution, and a clear peak is observed at Higgs boson mass(h^0). This peak can been seen with more than 5σ-significance in a wide parameter region as shown in Fig. 16(b). Events in this peak can be used for reconstruction of decay chain including $\tilde{\chi}_2^0$ as mentioned later. Events with $\tilde{\chi}_2^0 \to Z^0\tilde{\chi}_1^0$ also can been used in the same manner.

Figures 17 show invariant mass distributions of same flavour opposite charge di-lepton($\ell = $ e, μ) system for the 3-body decay of $\tilde{\chi}_2^0$. This decay mode becomes dominant, when the mass difference between $\tilde{\chi}_2^0$ and $\tilde{\chi}_1^0$ is smaller than M_Z. Sharp kinematic edges($M_{\ell\ell}^{max}$) are observed in both parameter points. Figure 15 shows the parameter region in which the $M_{\ell\ell}^{max}$ can be determined with L=100 fb^{-1}. $M_{\ell\ell}^{max}$ originated from 3-body decay can be observed in wide region. $M_{\ell\ell}^{max}$ is related to mass difference between $\tilde{\chi}_2^0$ and $\tilde{\chi}_1^0$, i.e.

$$M_{\ell\ell}^{max} = m(\tilde{\chi}_2^0) - m(\tilde{\chi}_1^0). \tag{3}$$

This kinematic edge can be determined very precisely as the same as 2-body decay case.

For $\ell^+\ell^-$ near the kinematic end point, momentum of $\tilde{\chi}_2^0$ in Lab-frame, $\vec{P}(\tilde{\chi}_2^0)$, can be directly reconstructed event by event, since $\ell^+\ell^-$ and $\tilde{\chi}_1^0$ almost stand still in $\tilde{\chi}_2^0$ rest-frame.

$$\vec{P}(\tilde{\chi}_2^0) = (1 + m(\tilde{\chi}_1^0)/m(\ell^+\ell^-))\vec{P}(\ell\ell) \tag{4}$$

Four-momentum of $\tilde{\chi}_2^0$ can be reconstructed assuming relation between m($\tilde{\chi}_1^0$) and m($\tilde{\chi}_2^0$), since mass difference between $\tilde{\chi}_1^0$ and $\tilde{\chi}_2^0$ is already measured from the kinematic edge.

Sharp peak is also observed at M_Z in right side of Fig. 17. This is contribution from the heavier state of chargino($\tilde{\chi}_2^\pm$) and neutralino($\tilde{\chi}_4^0$). When m_0 is much larger than $m_{1/2}$, Higgsino mass ($|\mu|$) is relatively small comparing Wino mass (otherwise, the Electroweak symmetry breaking has problem), then the resultant mass eigenstates of chargino and neutralino become the mixed states of Higgsinos and Wino. In such a case, there is substantial branching fraction of $\tilde{g} \to \tilde{\chi}_2^\pm f\bar{f}$, and Z^0 are produced from $\tilde{\chi}_2^\pm$. Momentum of the reconstructed Z^0 carries an information about mass of the parent chargino, $\tilde{\chi}_2^\pm$. Since a mean value of p_T^Z, $< p_T^Z >$, is proportional to the $\tilde{\chi}_2^\pm$ mass, it can be determined by the fitted $< p_T^Z >$ with an accuracy of 3% including systematic errors.
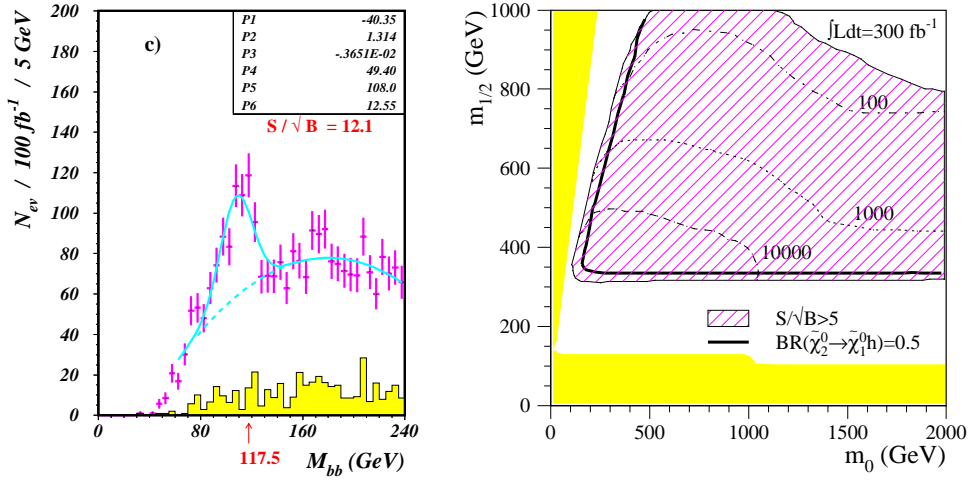
Figure 16: (a) Invariant mass distribution for $b\bar{b}$ system for $\tan\beta = 10$ ($m_0 = m_{1/2} = 500$ GeV and $\mu < 0$). Hatched histogram shows the background contribution from the standard model processes. (b) 5σ-visibility contour in m_0-$m_{1/2}$ plane for $\tan\beta = 10$ with luminosity of 300 fb^{-1}.
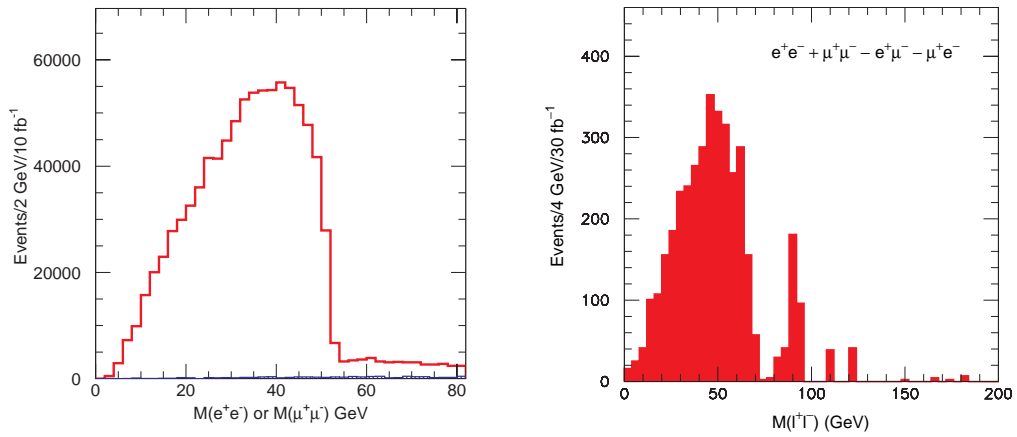
Figure 17: Invariant mass distributions for di-lepton system (e^+e^- and $\mu^+\mu^-$) Left histogram shows the case of small m_0 (at LHC point 3) and right shows large m_0 (at LHC point 4).
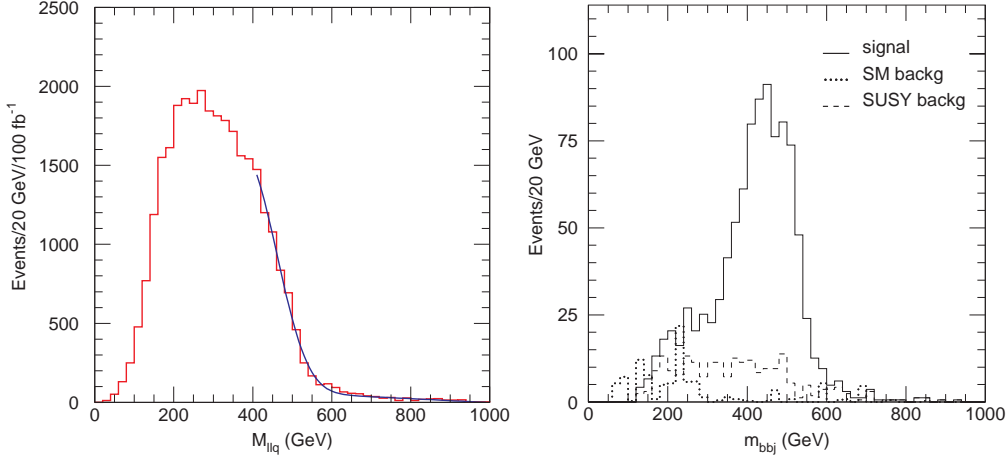
Figure 18: (a) Invariant mass distributions of q$\ell\ell$ (at LHC point 5). (b) Invariant mass distributions of qbb (at LHC point 1).

3.3.2 Kinematic end points of jets plus $\tilde{\chi}_2^0$:

$\tilde{\chi}_2^0$ is emitted mainly from $\tilde{q}_L \rightarrow q\tilde{\chi}_2^0$ and $\tilde{g} \rightarrow q\bar{q}\tilde{\chi}_2^0$ processes as presented in table 2. An information about mass of the parent particles, $\tilde{q}_L$ and $\tilde{g}$, can be obtained as follows.

$$\tilde{q}_L \rightarrow \tilde{\chi}_2^0 q$$
$$\rightarrow \tilde{\ell}^\pm \ell$$
$$\rightarrow \tilde{\chi}_1^0 \ell \text{ (2-body decay chain)}$$
$$\rightarrow \ell\ell\tilde{\chi}_1^0 \text{ (3-body decay)}$$
$$\rightarrow h\tilde{\chi}_1^0$$
$$\rightarrow b\bar{b} \text{ (h decay)}$$

are the leading decay chains of $\tilde{q}_L$. Figures 18 show invariant mass distributions of q$\ell\ell$- and qbb-systems. Although distributions are smeared by the limited energy resolution for hadron jets, these distributions have kinematic end points. Effects of the energy resolution and gluon emission from q should be taken into account to determine the end point. These kinematic end points are related to

$$M_{\ell\ell q}^{max} = \frac{\sqrt{m(\tilde{q}_L)^2 - m(\tilde{\chi}_2^0)^2}\sqrt{m(\tilde{\chi}_2^0)^2 - m(\tilde{\chi}_1^0)^2}}{m(\tilde{\chi}_2^0)}$$

$$(M_{hq}^{max})^2 = m(h)^2 + \frac{m(\tilde{q}_L)^2 - m(\tilde{\chi}_2^0)^2}{2m(\tilde{\chi}_2^0)^2}$$

$$\times \left(m(\tilde{\chi}_2^0)^2 + m(h)^2 - m(\tilde{\chi}_1^0)^2 + \sqrt{(m(\tilde{\chi}_2^0)^2 - m(h)^2 - m(\tilde{\chi}_1^0)^2)^2 - 4m(h)^2 m(\tilde{\chi}_1^0)^2} \right) \quad (5)$$

and can be determined with an accuracy of a few %.

For 3-body decay of $\tilde{\chi}_2^0$, four-momentum of $\tilde{\chi}_2^0$ can be directly reconstructed assuming the relation between m($\tilde{\chi}_1^0$) and m($\tilde{\chi}_2^0$) as already mentioned. An Invariant mass distribution of jet and reconstructed $\tilde{\chi}_2^0$ is shown in Fig. 19. A peak appears at $m(\tilde{q}_L)$ and this can be determined directly with an accuracy of 5% including systematic errors.

There are four unknown masses ($\tilde{q}_L$, $\tilde{\chi}_2^0$, $\tilde{\ell}^\pm$ and $\tilde{\chi}_1^0$) in the following 2-body decay chain:
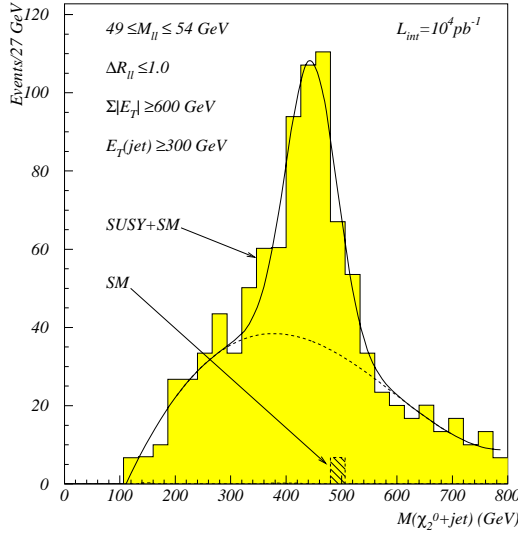
Figure 19: Invariant mass distribution of jet and the reconstructed $\tilde{\chi}_2^0$ for m_0= 300 GeV, $m_{1/2}$= 150 GeV and $\tan\beta$=2. Dotted line shows combinatorial background.

$$\tilde{q}_L \rightarrow \tilde{\chi}_2^0 q$$
$$\rightarrow \tilde{\ell}^{\pm}\ell$$
$$\rightarrow \tilde{\chi}_1^0 \ell \ ,$$

which is dominant mode in the parameter space of $m_0 < 0.8 m_{1/2}$. Figure 14(a), 18(b) and 20 show the invariant mass distributions of $\ell\ell$, $\ell\ell$+jet, and ℓ+jet. Three kinematic end points and one threshold of 4-body system ($\ell^+\ell^- q\tilde{\chi}_1^0$) are observed in these figures, and **all four unknown masses can be determined model-independently.** Although errors of these determined masses are strongly correlated, accuracies of these masses are 3, 6, 9 and 12% for $m(\tilde{q}_L), m(\tilde{\chi}_2^0), m(\tilde{\ell}^{\pm})$ and $m(\tilde{\chi}_1^0)$, respectively. We can examine SUSY model using the model-independent measurement [30]. Furthermore, there is one more constraint from $A_{\ell\ell}$ defined in eq.(2). Thus four unknown masses can be fitted with five constraints(1C fit) for this 2-body decay chain.

Following decay chains of $\tilde{g}$ is used to obtain an information about $\tilde{g}$ mass.
$$\tilde{g} \rightarrow \tilde{\chi}_2^0 q\bar{q}$$
$$\rightarrow \ell\ell\tilde{\chi}_1^0$$
$$\rightarrow \tilde{\chi}_1^{\pm} q\bar{q}$$
$$\rightarrow \ell\nu\tilde{\chi}_1^0$$

Four high p_T jets and three leptons are required to select $\tilde{g}\tilde{g}$ events. Figure 21 shows the invariant mass distribution of two high p_T jets. Since $\tilde{\chi}_2^0$ and $\tilde{\chi}_1^{\pm}$ are almost always nearly degenerate [16], the end point of M_{jj} is observed at the mass difference between $\tilde{g}$ and $\tilde{\chi}_2^0/\tilde{\chi}_1^{\pm}$. This can be determined with an accuracy of 1.5%. Main systematic error comes from uncertainty of calibration of jet energy scale (1%). Three masses of $\tilde{g}$, $\tilde{\chi}_2^0(\tilde{\chi}_1^{\pm})$ and $\tilde{\chi}_1^0$ can be determined assuming the relation between $m(\tilde{\chi}_1^0)$ and $m(\tilde{\chi}_2^0)$.

Dominant decay mode of $\tilde{q}_R$ is $\tilde{q}_R \rightarrow q\tilde{\chi}_1^0$. Kinematic end point of p_T distribution of the highest p_T-jet is related to $m(\tilde{q}_R)$, since p_T^{max} is proportional to $\frac{1}{2}m(\tilde{q}_R)(1 - (m(\tilde{\chi}_1^0)/m(\tilde{q}_R))^2)$ in $\tilde{q}_R$ rest-frame, and since $(m(\tilde{\chi}_1^0)/m(\tilde{q}_R))^2$ is expected to be small. $m(\tilde{q}_R)$ can be determined with an accuracy of a few %.
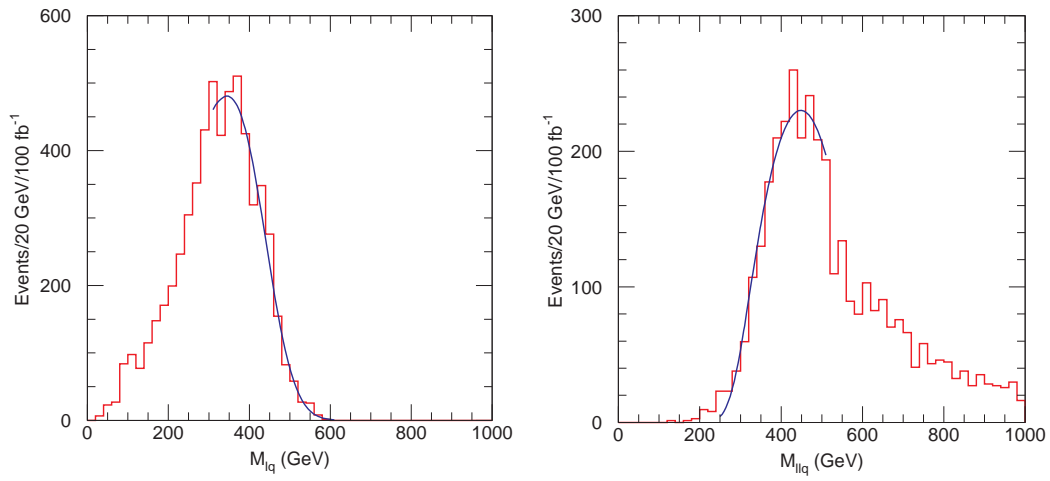
Figure 20: Invariant mass distributions of qℓ and qℓℓ (at LHC point 5).
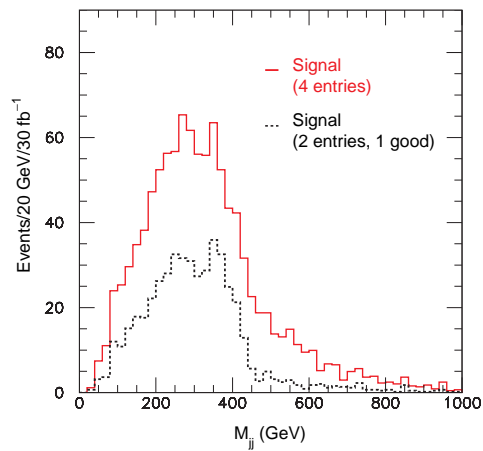
Figure 21: Invariant mass distributions of two jets (at LHC point 4). Solid line shows all combinations. Combinations of two hardest jets and two softest jets are rejected to obtained correct combinations (dotted line).
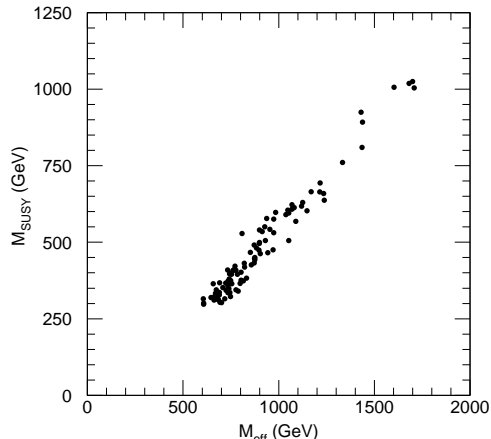
Figure 22: X-axis is fitted value of the peak of $\not{E}_T + \sum_{jets} p_T$ distribution. Y-axis is $\min(m(\tilde{q}_R), m(\tilde{g}))$. This relation is obtained in mSUGRA model.

Table 4: Determination of mSUGRA parameters (L=30 fb^{-1}): 'D' and 'ND' mean 'determined' and 'not determined',respectively.

LHC point	m_0 (GeV)	$m_{1/2}$ (GeV)	A_0 (GeV)	$\tan\beta$	$\text{sign}(\mu)$
1	400±100	400±10	ND	2.0±0.08	D
2	400±100	400±10	ND	10.0±2.0	D
3	200±10	100±1	ND	2.0±0.05	D
4	800±50	200±4	ND	10.0±2.0	D with
					L=300 fb^{-1}
5	$100^{+4.1}_{-2.2}$	300±2.7	ND	2.0±0.1	D
6	236±37	200±14	ND	41±3.9	ND

Min$(m(\tilde{q}), m(\tilde{g}))$ can be also determined by inclusive study. $\not{E}_T + \sum_{jets} p_T$ is proportional to $\min(m(\tilde{q}_R), m(\tilde{g}))$ as shown in Fig. 22. It can be determined independently from the exclusive studies mentioned above. Accuracy is about 15% [26] including systematic errors, and large contributions comes from the uncertainty of $\not{E}_T + \sum_{jets} p_T$- distribution for the background processes.

3.4 Summary and comments on mSUGRA

$\tilde{\chi}_2^0$ plays important role to determine masses of the SUSY particles, and studies has been done systematically [12,27] for various decay modes presented in table 3. $\tilde{g} \to q\bar{q}\tilde{\chi}_2^0(\tilde{\chi}_1^\pm)$ and $\tilde{q} \to q\tilde{\chi}_{1,2}^0$ processes are useful to determine $\tilde{g}$ or $\tilde{q}$ mass as presented in Sec.3.3. Although all of $\tilde{g}$-, $\tilde{q}_{L/R}$-, $\tilde{\ell}^\pm$-, $\tilde{\chi}_2^0$- and $\tilde{\chi}_1^0$-mass can not be determined independently, many parts of the mSUGRA parameters can be determined [12] by global fit using these measurements on these end points, since there are strong correlations between these masses in the mSUGRA model. Fitted values of the mSUGRA parameters are summarised in table 4 for various LHC points. As mentioned in Sec.3.1, $m_{1/2}$ is determined mainly by $m(\tilde{\chi}_2^0)$ and $m(\tilde{g})$, and it's error is smaller than 10%. $m(\tilde{q}_L)$ and $m(\tilde{\ell}_R^\pm)$ contribute to strong constraint on m_0, whose accuracy is 5-20%. $\tan\beta$ is determined by Higgs boson mass.

When $|\mu|$ mass is not larger than wino mass ($\sim 0.8 m_{1/2}$), the heavier states of chargino and

neutralino also appear in the cascade decay chain of q̃ and g̃. Substantial branching fraction including $\tilde{\chi}_2^\pm$ and $\tilde{\chi}_4^0$;

$$\tilde{q} \rightarrow \tilde{\chi}_2^\pm / \tilde{\chi}_4^0 + q$$
$$\rightarrow \tilde{\chi}_2^0 / \tilde{\chi}_1^\pm + Z^0 / W^\pm$$
$$\rightarrow \tilde{\chi}_1^0 + f\bar{f}$$

is expected in this case. Event topology of such a decay chain is more complicated, but it is a good chance to measure $|\mu|$ directly. $|\mu|$ is important, since Higgsino plays important role to the Electroweak symmetry breaking in Supersymmetry. It is necessary to study systematically decay chains involving $\tilde{\chi}_2^\pm$ and $\tilde{\chi}_4^0$.

Situations of 3rd generation $\tilde{q}$ ($\tilde{t}$ and $\tilde{b}$) are complicated but very important because of the following two reasons:

- These masses depend not only on m_0 and $m_{1/2}$ but also on A_0, $\tan\beta$, and μ. Mass spectrum change drastically, then there are many decay pattern of $\tilde{t}$ and $\tilde{b}$ to be considered. Systematic study on the decay patterns is necessary, and the observed decay patterns will help us to understand A_0, $\tan\beta$, and μ.

- $\tilde{t}$ and $\tilde{b}$ have large coupling to Higgsino, since Y_t and $Y_b(\tan\beta \gg 1)$ is very large. Then $\tilde{\chi}_2^\pm$ and $\tilde{\chi}_{3,4}^0$ appear in the decay chains, if kinematically possible. Event topology is more complicated than that of 1st and 2nd generations, but it is good chance to study Higgsino at LHC. It may have key of the Electroweak symmetry breaking in Supersymmetry.

4   Electroweak physics

High precision measurements on Z^0 and $W^\pm$ have been performed at LEP and SLD, and the Electroweak theory has experienced severe test for the last ten years. It still passes this test as shown in Fig. 23, since there are three parameters which are not yet well determined. Higgs boson has been still missing link, and its mass is an unknown parameter in the Electroweak theory. As mentioned in Sec. 2, the standard model Higgs boson should be discovered at LHC, if it exists, and its mass can be determined with an accuracy of 0.2%.

The solid contour shows the allowed region(68% C.L.) on m_{top}-m_W plane, it still has cross to the directly determined region of m_{top} and m_W. Current errors on m_{top} and m_W are 5 GeV and 34 MeV [g], respectively. It is very important to determine precisely m_{top} and m_W in order to perform the final examination of the Electroweak theory.

4.1   Top quark

The LHC will be a top factory with 10^7 $t\bar{t}$ events [h] per year at a low luminosity of $10^{33}cm^{-2}s^{-1}$. This number is much larger by factor 2×10^4 than that at Tevatron Run-Ib, which has already presented the high performance for study of top quark at hadron colliders.

The top mass can be reconstructed using three jets system from $t\bar{t} \rightarrow (\ell\nu b)(jjb)$ final state. High p_T lepton, which is produced from one $W^\pm$, is used as a trigger signal, and three jets system(jjb) are produced from top quark decay. Although there is ambiguity in choice of B-jet, the correct combination is naturally enhanced by selecting B-jet near jj-system, since the produced top quarks have large p_T at LHC. Figures 24 shows the invariant mass distributions for the jj and jjb system. The wrong combinations are shown with hatched histogram in these figures. Uncertainties of the reconstructed mass are summarised in table 5. Top mass will be determined with an accuracy of 1%. Calibration of the energy scale on hadronic jet

---

[g]62 MeV at Tevatron Run-Ib and 40 MeV at LEP-II

[h]The production cross-section is 833 pb with the NLO calculation at 14 TeV.
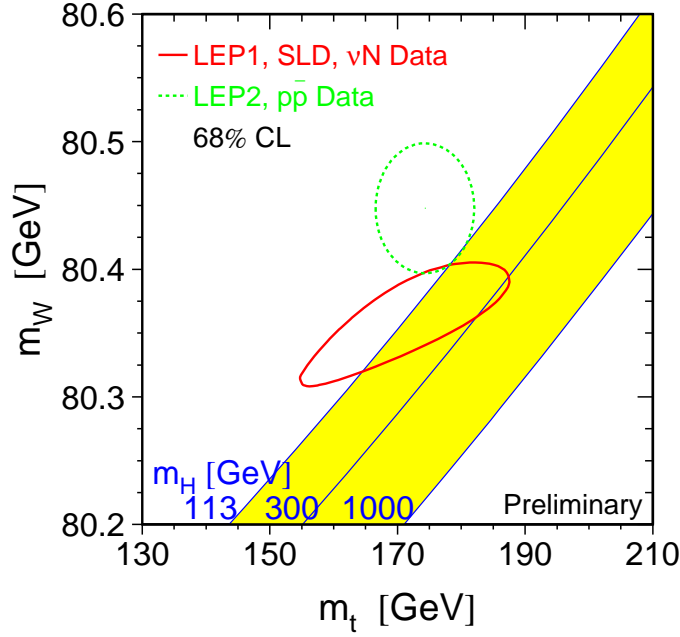
Figure 23: Current status (2001 winter) of the Electroweak physics.

Table 5: Summary of errors on the determination of top quark mass with L=10 fb^{-1}:

Source	error (GeV)
Statistic	0.2
Energy scale of hadron calorimeters	1.1
fragmentation of b quark	0.3
FSR g emission	1.2
Background (wrong combination)	0.2
TOTAL	1.7 GeV

(especially B-jet) is important. Jets of the light flavour and gluon are calibrated using the $q\gamma$ and $g\gamma$ processes. The Energy scale correction on B-jet is difficult, since the ν is emitted in the semi-leptonic decay of the bottom quark. This correction should be estimated by the average energy of ν, but uncertainties of this effect is the large systematic error on $M_{\rm t}$. Second largest systematic error is due to the effect that the energetic gluon emits in the final state.

Kinematic fit improves the accuracy of measurement on top quark mass. Following four constraints are used to calculate χ^2 of fit.

- $M_{jj}=M_{\rm W^{\pm}}^{PDG}$

- $M_{\ell\nu}=M_{\rm W^{\pm}}^{PDG}$

- $M_{jj{\rm b}}=M_{\rm t}^{fit}$

- $M_{\ell\nu{\rm b}}=M_{\rm t}^{fit}$

χ^2 is required to be smaller than 4, and the fit efficiency is estimated to be about 80%. $M_{\rm t}^{fit}$ has a linear relation to χ^2, i.e $M_{\rm t}^{fit} = A + B \times \chi^2$. $M_{\rm t}$ will be obtained with an extrapolation to $\chi^2 \to 0$.
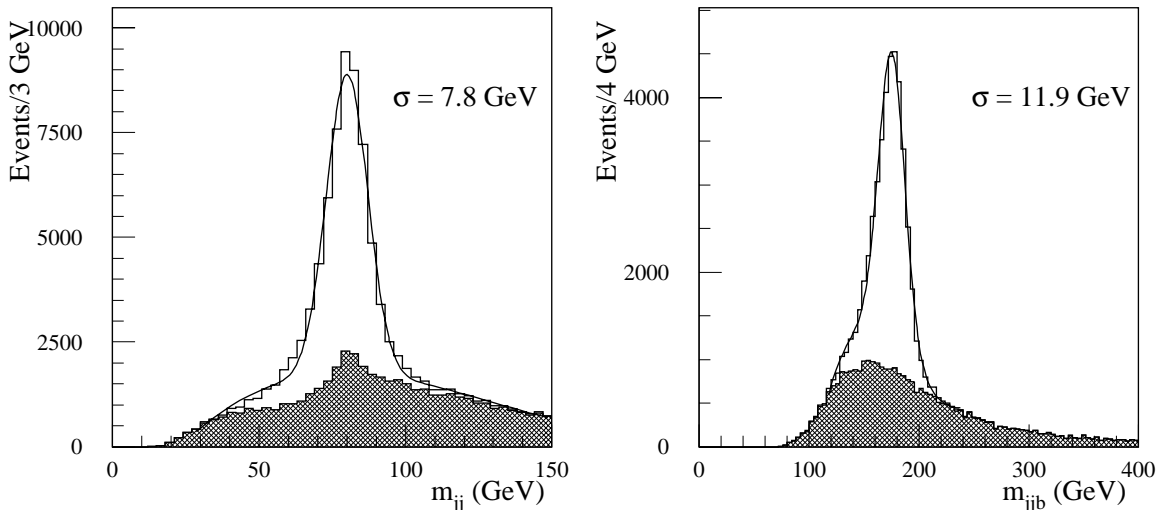
Figure 24: Invariant mass distributions for (a) selected jj pair and (b) jjb with L=10 fb^{-1}. The hatched histograms show the wrong combinations.

Table 6: Sensitivities of the exotic decay modes of top quark with L=300 fb^{-1}, typical predictions in the SUSY models and in the SM are also listed.

Exotic decay mode	Sensitivity on branching fraction	Prediction in SUSY	Prediction in SM
t → bH$^+$	0.03		0
t → qZ^0	10^{-4}	$\sim 10^{-4}$	$\sim 10^{-13}$
t → qγ	10^{-4}	$\sim 10^{-5}$	$\sim 10^{-13}$
t → qg	10^{-2}	$\sim 10^{-3}$	$\sim 10^{-11}$

There are two major reasons to make χ^2 worse, and they are related to two largest systematic errors shown in table 5. First is that an energy of ν emitted from the b is far way from an average correction of B-jet. It is one of main source of uncertainties on the energy scale of hadron, and can be reduced to 0.7 GeV using this extrapolation. Second reason is that a hard FSR gluon exists in the final state, and this effect is the largest error in table 5. Its effect also can be drastically reduced to 0.2 GeV with the extrapolation. The total error on the measured M_{t} becomes 0.8 GeV finally at LHC.

The large number of t$\bar{\text{t}}$ provides sensitivity to non standard decays of the t quark. In the standard model, top quark decay into bW$^\pm$ with a fraction of almost 100%. On the other hand, exotic decay modes, especially flavour changing decay, are expected in the SUSY models. The sensitivities of the various decay modes are summarised in table 6.

5 Conclusions

The standard Higgs boson should be discovered at LHC with just integrated luminosity of 10fb^{-1} at each detector, if it exists less than 1 TeV. We can perform a critical test on the Higgs mechanism. H$^0_{SM} \to \gamma\gamma$, t$\bar{\text{t}}$H$^0_{SM}(\to$ b$\bar{\text{b}})$ and ZZ$(\to \ell^+\ell^-\ell^+\ell^-)$ play important role for the discovery. Its mass and natural decay width can be determined precisely using these modes.

LHC has also a good potential for the MSSM higgs bosons. The lighter higgs, h^0, will be discovered in any parameter space, and we can determine a mass of h^0 as the same as H$^0_{SM}$. H^0,

A^0 and $H^\pm$ will be also discovered if these masses are lighter than 1 TeV, and if $\tan\beta$ is larger than about 10.

Measurements of the couplings between (SM, MSSM) Higgs boson(s) and fermions/Gauge bosons will give the direct informations of origin of "Mass", and it will give the first evidence of Yukawa couplings. Careful investigations of this business are going under way.

Supersymmetry should be discovered at LHC, if $\tilde{g}$ and $\tilde{q}$ are lighter than about 2.5 TeV. Signals will be, perhaps, found not only in the ($\not{E}_T$ + jets) channel but also in ($\not{E}_T$ + jets + lepton(s)) channels. Exclusive studies have been performed. $\tilde{\chi}_2^0$ plays important role to determine masses of the SUSY particles, and studies has been done systematically. In many cases, it should be possible to measure many combinations of masses of SUSY particles from various kinematic distributions. Masses of $\tilde{g}$, $\tilde{q}$, $\tilde{\ell}^\pm$, $\tilde{\chi}_2^0$ and $\tilde{\chi}_1^0$ can be determined with help of model. Accuracies of these masses are about a few–10%. When there are at least three 2-body decay chain, masses can be determined model-independently.

Event topologies involving 3rd generation are complicated, but these will provide good knowledges about Higgsino and trilinear coupling. Furthermore, measurements of decay branching fractions will give redundant informations of SUSY parameters, and redundancy is very important to examine the SUSY models. Systematic studies on both subjects are necessary.

LHC will be a top factory and has a good potential on the various properties of top quark.

References

1. http://lhc.web.cern.ch/lhc/
2. ATLAS Technical proposal, CERN/LHCC/94-43.
3. CMS Technical proposal, CERN/LHCC/94-38.
4. ATLAS Physics TDR vol.1 , CERN/LHCC/99-15.
5. http://cmsdoc.cern.ch/cms/TDR/
6. M. Spira, hep-ph/9705337. There are also the detail calculations of K-factor in this reference.
7. T. Plehn, D. Rainwater and D. Zeppenfeld, Phys. Lett. **B454** (1999) 297-303.
8. A. Djouadi, J. Kalinowski and M. Spira, Comput. Phys. Commun. **108** (1998) 56-74.
9. http://lepewwg.web.cern.ch/LEPEWWG/plots/winter2001/
10. F. Gianotti, Presented at LHCC open session 5/7/2000,
    http://atlasinfo.cern.ch/Atlas/GROUPS/PHYSICS/HIGGS/higgs-www/LHCC-talks/lhcc.pdf
11. V. Drollinger, Th. Muller and D. Denegri, hep-ph/0111312.
12. ATLAS Physics TDR vol.2 , CERN/LHCC/99-15.
13. T. Plehn, D. Rainwater and D. Zeppenfeld, Phys. Rev. **D61** (2000), 093005.
14. M. Spira at al, hep-ph/9504378.
15. D. Zeppenfeld, R. Kinnunen, A. Nikitenko, R. Was, Phys. Rev. **D62** (2000) 013009.
16. General Reviews: H.P. Nilles, Phys. Rep. **110** (1984) 1
    H.E. Haber and G.L. Kane, Phys. Rep. **117** (1985) 75.
17. General Reviews: G. Jungman, M. kamionkowski and K. Griest, Phys. Rept. **267** (1996) 195.
18. S. Abel et al., hep-ph/0003154 for review
    L. Alvarez-Gaume, J. Polchinski and M.B. Wise, Nucl. Phys. **B221** (1983) 495
    L. Ibanez, Phys. Lett. **B118** (1982) 73
    J. Ellis, D.V. Nanopolous and K.Tamvakis, Phys. Lett. **B121** (1983) 123.
19. M. Dine, W. Fischler and M. Srednicki, Nucl. Phys. **B189** (1981) 575
    S. Dimopoulos and S. Raby, Nucl. Phys. **B192** (1981) 353
    C. Nappi and B. Ovrut, Phys. Lett. **B113** 175

L. Alvarez-Gaume, M. Claudson and M.B. Wise, Nucl. Phys. **B207** (1982) 961

M. Dine and A.E. Nelson, Phys. Rev. **D48** (1993) 1227

M. Dine, A.E. Nelson and Y. Shirman, Phys. Rev. **D51** (1995) 1362

M. Dine et al., Phys. Rev. **D53** (1996) 2658

20. P. Fayet, Phys. Lett. **B69** (1977) 489.
21. M. Drees and K. Hikasa, Phys. Lett. **B252** (1990) 127
    K. Hikasa and M. Kobayashi, Phys. Rev. **D36** (1987) 724
    A. Bartl, W. Majerotto and W. Porod, Z. Phys. **C64** (1994) 499.
22. E. Eichten et al., Rev. Mod. Phys. **56** (1984) 579.
23. M. Spira, Nucl. Phys. Proc. Suppl. **89** (2000) 222.
24. H. Baer, F.E. Paige, S.D. Protopopescu and X. Tata, hep-ph/0001086 (2000).
25. S. Mrenna, Comp. Phys. Comm. **101** (1997) 232
    T. Sjöstrand, Comp. Phys. Comm. **82** (1994) 74.
26. D.R. Tovey, Phys. Lett. **B498** (2001) 1.
27. S. Abdullin et al., CMS/Note/98-006, hep-ph/9806366.
28. M. Nojiri, D. Toya, and T. Kobayashi, Phys. Rev. **D62** (2000) 075009.
29. By A. Djouadi, Y. Mambrini and M. Muhlleitner Eur. Phys. J. **C20** (2001) 563.
30. B.C. Allanach, C.G. Lester, M.A. Parker and B.R. Webber CERN-TH-2000-149 (2000).